

1 **Distinguishing between old and modern permafrost sources in the Northeast**
2 **Siberian land-shelf system with compound-specific $\delta^2\text{H}$ analysis**

3
4 Jorien E. Vonk¹, Tommaso Tesi^{2,3}, Lisa Bröder^{2,4}, Henry Holmstrand^{2,4}, Gustaf
5 Hugelius^{4,5}, August Andersson^{2,4}, Oleg Dudarev^{6,7}, Igor Semiletov^{6,7,8}, Örjan
6 Gustafsson^{2,4}

7
8 ¹ Department of Earth Sciences, VU University, The Netherlands

9 ² Department of Environmental Science and Analytical Chemistry, Stockholm
10 University, Sweden

11 ³ ISMAR Institute of Marine Sciences, Bologna, Italy

12 ⁴ Bolin Centre for Climate Research, Stockholm University, Sweden

13 ⁵ Department of Physical Geography, Stockholm University, Sweden

14 ⁶ Pacific Oceanological Institute FEBRAS, Vladivostok, Russia

15 ⁷ Tomsk Polytechnic University, Tomsk, Russia

16 ⁸ University of Alaska Fairbanks, Fairbanks, USA

17
18 Correspondence to: Jorien Vonk (j.e.vonk@vu.nl)

19
20
21 **Keywords:** deuterium isotopes, yedoma, ice complex deposit, n-alkanoic acids, n-
22 alkanes, organic matter, stable carbon isotopes, radiocarbon, Siberian Arctic,
23 sediments, permafrost thaw

24
25 **Abstract**

26 Pleistocene ice complex permafrost deposits contain roughly a quarter of the organic
27 carbon (OC) stored in permafrost terrain. When permafrost thaws, its OC is
28 remobilized into the (aquatic) environment where it is available for degradation,
29 transport or burial. Aquatic or coastal environments contain sedimentary reservoirs
30 that can serve as archives of past climatic change. As permafrost thaw is increasing
31 throughout the Arctic, these reservoirs are important locations to assess the fate of
32 remobilized permafrost OC.

33 We here present compound-specific deuterium ($\delta^2\text{H}$) analysis on leaf waxes as a tool
34 to distinguish between OC released from thawing Pleistocene permafrost (Ice
35 Complex Deposits; ICD) and from thawing Holocene permafrost (from near-surface
36 soils). Bulk geochemistry (%OC, $\delta^{13}\text{C}$, %total nitrogen; TN) was analyzed as well as
37 the concentrations and $\delta^2\text{H}$ signatures of long-chain *n*-alkanes (C_{21} to C_{33}) and
38 mid/long-chain *n*-alkanoic acids (C_{16} to C_{30}) extracted from both ICD-PF samples
39 ($n=9$) and modern vegetation/O-horizon (Topsoil-PF) samples ($n=9$) from across the
40 northeast Siberian Arctic.

41 Results show that these Topsoil-PF samples have higher %OC, higher OC/TN values,
42 and more depleted $\delta^{13}\text{C}$ -OC values than ICD-PF samples, suggesting that these former
43 samples trace a fresher soil and/or vegetation source. Whereas the two investigated
44 sources differ on the bulk geochemical level, they are, however, virtually
45 indistinguishable when using leaf wax concentrations and ratios.

Deleted: Median concentrations of high-molecular weight *n*-alkanes (sum of C_{25} - C_{27} - C_{29} - C_{31}) were 210 ± 350 $\mu\text{g/gOC}$ (median \pm IQR) for Topsoil-PF and 250 ± 81 $\mu\text{g/gOC}$ for ICD-PF samples. Long-chain *n*-alkanoic acids (sum of C_{22} - C_{24} - C_{26} - C_{28}) were more abundant than long-chain *n*-alkanes, both in Topsoil-PF samples (4700 ± 3400 $\mu\text{g/gOC}$) and in ICD samples (6630 ± 3500 $\mu\text{g/gOC}$).

53 However, on the molecular-isotope level, leaf wax biomarker $\delta^2\text{H}$ values are
54 statistically different between Topsoil-PF and ICD-PF. For example, the mean $\delta^2\text{H}$
55 value of C_{29} *n*-alkane was $-246 \pm 13\text{‰}$ (mean \pm stdev) for Topsoil-PF and $-280 \pm 12\text{‰}$
56 for ICD-PF. With a dynamic isotopic range (difference between two sources) of 34 to
57 50‰, the isotopic fingerprints of individual, abundant, biomarker molecules from
58 leaf waxes can thus serve as end-members to distinguish between these two sources.
59 We tested this molecular $\delta^2\text{H}$ tracer along with another source-distinguishing
60 approach, dual-carbon ($\delta^{13}\text{C}-\Delta^{14}\text{C}$) isotope composition of bulk OC, for a surface
61 sediment transect in the Laptev Sea. Results show that general offshore patterns
62 along the shelf-slope transect are similar, but the source apportionment between the
63 approaches vary, which may highlight the advantages of either. This study indicates
64 that the application of $\delta^2\text{H}$ leaf wax values has potential to serve as a complementary
65 quantitative measure of the source and differential fate of OC thawed out from
66 different permafrost compartments.
67

Deleted: T

Deleted: , whereas the C_{31} *n*-alkane was $-247 \pm 23\text{‰}$ for Topsoil-PF and $-297 \pm 15\text{‰}$ for ICD-PF. The C_{28} *n*-alkanoic acid $\delta^2\text{H}$ value was $-220 \pm 15\text{‰}$ for Topsoil-PF and $-267 \pm 16\text{‰}$ for ICD-PF.

Deleted: The $\delta^2\text{H}$ molecular approach has the advantage that it circumvents uncertainties related to a marine end-member, yet the $\delta^{13}\text{C}-\Delta^{14}\text{C}$ approach has the advantage that it represents the bulk OC fraction thereby avoiding issues related to the molecular-bulk upscaling challenge.

78 **1 Introduction**

79 Climate warming is causing permafrost soils to thaw, exposing its organic matter
80 (OM) to decomposition (e.g., Schuur et al., 2015; Zimov et al., 1993; Semiletov et al.,
81 2012). Thaw will increase the hydrological connectivity of landscapes and will cause
82 release of OM into the aquatic environment (Walvoord et al., 2012; Vonk et al., 2015;
83 Anderson et al., 2011). Here, the OM can continue to decompose, generating
84 greenhouse gases (e.g., Semiletov et al., 1996a,b; Anderson et al., 2009; Shakhova et
85 al., 2015), or be destined for burial in inland and coastal sediments. These
86 sedimentary archives serve as long- and short-term reservoirs that attenuate
87 greenhouse gas emissions from thawing permafrost (Vonk and Gustafsson, 2013;
88 Semiletov et al., 2011).

Deleted: to

89
90 The release of OM from thawing permafrost into aquatic sediments varies over time
91 and space. A recent study showed that at the end of the last glacial, the surface active
92 layer of terrestrial permafrost released about 4.5 Tg organic carbon (OC) per year
93 from just the Lena watershed onto the nearby shelf, whereas current annual OC
94 release is estimated to be only about a tenth of this (Tesi et al., 2016). In addition to
95 active layer material, OM from deeper and older permafrost sources can also thaw
96 and be released into the environment (Shakhova et al., 2007, 2014). This process
97 currently dominates the delivery of terrestrial material onto the East Siberian Arctic
98 shelf (Vonk et al., 2012; Semiletov et al., 1999) and is expected to increase due to
99 accelerating coastal erosion rates (Günther et al., 2013).

100
101 Different permafrost OC stocks exhibit variable vulnerabilities to thaw remobilization
102 (Schuur et al., 2015). In addition to a subsea permafrost OC stock, soils and sediments
103 of the terrestrial northern permafrost zone store about 1300±200 Pg OC, with
104 separate upscaling approaches applied for soil stocks (0-3m depth), deltaic sediments
105 (full depth) and Yedoma sediments (full depth) (Hugelius et al., 2014). Yedoma
106 sediments, a.k.a. Ice Complex Deposits (ICD) are polygenetic, ice-rich Pleistocene-
107 aged deposits that are present in the unglaciated parts of Siberia and Alaska
108 (Schirrmeister et al., 2011). These deposits contain roughly a quarter of the OC stored
109 in permafrost terrain, but estimates vary from ca. 200-400 Pg C (Strauss et al., 2013;
110 Schuur et al., 2015). The presence of massive ice wedges in ICD causes landscapes to
111 collapse upon thaw, exposing deeper stocks of OC. This type of relatively abrupt thaw
112 is increasing in many parts of the arctic landscape (Schuur et al., 2015). At the same
113 time, deepening of the active layer causes gradual thaw that occurs across entire
114 landscapes (Shiklomanov et al., 2013).

115
116 With a tool to detect and monitor different types of permafrost OM in coastal
117 environments, one could assess (historical and spatial) variability in permafrost
118 source input, degradation and thaw, as well as the relative degradation of different
119 permafrost types. For example, the relative release of OC from ICD versus topsoil
120 permafrost has earlier been distinguished and quantified through the use of dual-
121 carbon isotopes ($\delta^{13}\text{C}$ and $\Delta^{14}\text{C}$) on bulk OC in the shelf environment of the Laptev
122 and East Siberian Sea. It was shown that topsoil permafrost OC dominates in
123 suspended particulate matter (Karlsson et al., 2011; 2016; Vonk et al., 2012) and ICD

125 permafrost OC dominates in the surface sediments (Vonk et al., 2012; Semiletov et al.,
126 2011; 2012). Vonk et al. (2014) further showed that topsoil OC is actively degraded
127 during horizontal transport whereas ICD permafrost OC rapidly settles. Winterfeld et
128 al. (2015) showed, using dual-carbon isotopes on riverine material, that suspended
129 particulate OC in the Lena Delta mostly consists of Holocene material instead of
130 material from ICD permafrost.

131
132 This $\delta^{13}\text{C}-\Delta^{14}\text{C}$ dual-carbon isotope approach carries the strong advantage that it
133 operates on the bulk OC level, thereby circumventing the "molecular-bulk upscaling
134 challenge". This challenge relates to issues associated with upscaling from the
135 molecular isotope level to the bulk level. These issues relate to the relative
136 concentration (*n*-alkanes and *n*-alkanoic acids represent only a fraction of the total
137 OC) but also to processes such as selective degradation, differences in physical
138 association, or dispersion differences. However, the $\delta^{13}\text{C}-\Delta^{14}\text{C}$ approach also has
139 drawbacks, such as a weak distinction between the $\delta^{13}\text{C}$ end-member values of
140 Topsoil-PF versus ICD-PF. Also, the marine $\delta^{13}\text{C}$ end member values in coastal Arctic
141 shelf waters are uncertain and may be more depleted than at mid-latitudes due to
142 uptake of relatively depleted dissolved CO_2 values caused by cold polar water
143 (Meyers, 1997; Tesi et al. *this special issue*) or degradation of terrestrial matter
144 (Anderson et al., 2009; 2011; Semiletov et al., 2013; 2016), generating a potential
145 overlap between marine and topsoil $\delta^{13}\text{C}$ end-members.

146
147 Here we propose a complementary tool to trace permafrost OC release into the
148 coastal environment based on molecular $\delta^2\text{H}$ analysis on leaf waxes. We will evaluate
149 the performance of this tool using additional geochemical data as well as the bulk
150 $\delta^{13}\text{C}-\Delta^{14}\text{C}$ mixing approach. Isotopes in water molecules ($\delta^2\text{H}$ or $\delta^{18}\text{O}$) in glacial ice
151 cores as well as in massive ground ice in the northern hemisphere have been used for
152 reconstructing palaeotemperatures (e.g., Kotler and Burn, 2000; Johnson et al., 2001;
153 Opel et al., 2011; Meyer et al., 2015; Wetterich et al., 2016) as the isotopic value of
154 local precipitation is a function of local climate (Craig, 1961; Sachse et al., 2004; Smith
155 and Freeman, 2006). Higher plants use water as their primary source of hydrogen
156 during photosynthesis (Sternberg, 1988). The $\delta^2\text{H}$ isotope values of leaf wax *n*-
157 alkanic acids or *n*-alkanes are therefore reflecting the $\delta^2\text{H}$ isotopic value of local
158 precipitation (e.g., Sachse et al., 2004; Sessions et al., 1999), after correction for the
159 net fractionation during biosynthesis, and evapotranspiration (Leaney et al., 1985).
160 Global precipitation values can vary immensely (Dansgaard, 1964), with values up to
161 +50‰ in Eastern Africa, but approaching -200‰ near the North Pole (www.iaea.org)
162 or even below -400‰ in Antarctica (i.e. SLAP2 standard, Standard Light Antarctic
163 Precipitation, is -427.5‰). Additionally, the fractionation between source water and
164 plant wax molecules varies both in time and space, and can be up to -170‰ (Smith
165 and Freeman, 2006; Sachse et al., 2004; Polissar and Freeman, 2010) but appears
166 relatively small at higher latitudes (between -59 and -96‰; Shanahan et al., 2013;
167 Wilkie et al., 2013; Porter et al., 2016). Differences in $\delta^2\text{H}$ signatures of leaf wax
168 molecules from terrestrial regions with different (past) climates could therefore
169 potentially be applied to derive the relative proportion of different types of thawing

- Deleted: proxies
- Formatted: Font:Italic
- Formatted: Font:Italic
- Deleted: that relate to upscaling from the molecular to the bulk level (e.g.
- Deleted:)

- Formatted: Font:12 pt
- Deleted: by as much as 200‰
- Formatted: Font:12 pt
- Deleted: around
- Deleted: 0
- Deleted: the tropics

178 permafrost in nearby coastal settings. Despite the plant fractionation associated with
179 kinetics and plant physiology (Sachse et al., 2012), we hypothesize that $\delta^2\text{H}$
180 signatures of leaf wax *n*-alkanoic acids and *n*-alkanes are more depleted in OC from
181 permafrost deposits formed during the colder Pleistocene (generally correlating with
182 ^2H -depleted precipitation), compared to more enriched values in OC from active layer
183 or surface permafrost formed during the warmer Holocene.

Deleted: We hypothesize

Deleted: and drier

Formatted: Superscript

184
185 This study investigates a source-specific $\delta^2\text{H}$ signature for both ICD permafrost and
186 recent, surface soil permafrost in Northeast Siberia. Furthermore, we explore the
187 possibilities of using these isotopic end-member values in regional source-
188 apportionment calculations that aim to quantify the relative contribution of different
189 sources of permafrost OC. As permafrost thaw progresses, particularly in ice-rich
190 permafrost such as ICD, it is increasingly important to trace the fate of remobilized
191 and decomposing OC in the Arctic environment. Our proposed tool may be used to
192 trace these temporal and spatial differences in OC release from permafrost thaw, as
193 well as the extent of burial of OC in sedimentary reservoirs.

194 195 **2 Methods**

196 197 **2.1 Sampling**

198 A total of 18 samples were collected throughout the Siberian Arctic. Recent surface
199 soils ($n=7$) and vegetation ($n=2$) samples were analyzed and (from here on) referred
200 to as the "topsoil" permafrost (Topsoil-PF) sample set, whereas ICD-PF samples were
201 obtained from ICD soil profiles ($n=7$) and suspended particulates from ICD
202 formations ($n=2$) (Fig. 1 and Table 1). Eight offshore sediments along a shelf-slope-
203 continental rise transect in the Laptev Sea were collected in 2014, further marine
204 sampling details can be found in Bröder et al. (2016b).

205
206 The Topsoil-PF samples represent O and A soil genetic horizons in sites with active
207 soil formation. The sites were chosen to represent typical soil and vegetation types
208 in the investigated permafrost landscapes, including both taiga and tundra sites.
209 Samples were collected by depth or soil horizon increments from open soil pits using
210 fixed volume sampling procedures.

211
212 The ICD-PF samples were collected from vertical exposures that were excavated to
213 expose intact permafrost. Fixed-volume samples were collected by coring
214 horizontally into the frozen sediments to extract ICD-PF samples from consecutive
215 depths.

216
217 For more details about sampling sites, including location, vegetation and soil types
218 see table 1 (terminology following the U.S.D.A. Soil Taxonomy; Soil Survey Staff,
219 2014). Sampling was done in late summer near the time of maximum annual active
220 layer depth, in July 2010 (ICD-8 and ICD-9; Vonk et al. (2013)) and August 2011
221 (Palmtag et al., 2015) for the Kolyma River region, in August 2012 for the lower Lena
222 River and Indigirka River (Siewert et al., 2015; Weiss et al., 2015) and in August 2013

Deleted: CH DY-3A and 4A

226 for the upper Lena River (Siewert et al., 2016). For more detailed descriptions of
227 sample collection we refer to these references. The vegetation samples **TS-8G (grass)**
228 and **TS-9G (grass)** were obtained from the tundra near Medvezhka River and a birch
229 forest near Y4 stream, respectively, in July 2012.

Deleted: CH

Deleted: Medv

Deleted: CH Y4

230
231 Samples **ICD-8** and **ICD-9** were obtained in July 2010 at the Duvannyi Yar ICD
232 exposure along the Kolyma River (Vonk et al., 2013). The particulate sediment
233 samples were taken from thaw streams that were freshly formed from thawing ICD
234 (transport time from thaw to sampling estimated to be less than 1h).

Deleted: CH DY-3A

Deleted: 4A

235 2.2 Analytical methods

236 Freeze-dried samples were extracted using an ASE 200 accelerated solvent extractor
237 (Dionex Corporation, USA) using DCM/MeOH (9:1 v/v) at 80°C (5x10⁶ Pa)
238 (Wiesenberg et al., 2004). After the extraction, solvent-rinsed activated copper and
239 anhydrous sodium sulfate were added to the extracts to remove sulfur and excess
240 water, respectively. After 24 h, extracts were filtered on pre-combusted glass wool
241 and concentrated with the rotary evaporator. Extracts were transferred into glass
242 tubes, evaporated to complete dryness and re-dissolved in 500 µl of DCM. Lipid
243 fractionation was performed via column chromatography using amino-propyl Bond
244 Elut (500 mg/3 ml) to retain the acid fraction and Al₂O₃ to separate the hydrocarbon
245 and polar fractions (Vonk et al., 2010).

246
247
248 Prior to the analyses, saturated *n*-alkanes (hydrocarbon fraction) were further
249 purified using 10% AgNO₃ coated silica gel to retain the unsaturated fraction. The acid
250 fraction was methylated using a mixture of HCl, MilliQ water and methanol at 80°C
251 overnight to obtain the fatty acid methyl ester (FAME) fraction. Methylated acids
252 were extracted with hexane and further purified using 10% AgNO₃ coated silica gel.
253 The hydrocarbon and FAME fractions were quantified via gas chromatography mass
254 spectrometry (GC-MS) in full scan mode (50-650 m/z) using the response factors of
255 commercially available standards (Sigma-Aldrich). The GC was equipped with a 30
256 m×250 µm DB5-ms (0.25 µm thick film) capillary GC column. Initial GC oven
257 temperature was set at 60°C followed by a 10°C min⁻¹ ramp until a final temperature
258 of 310°C (hold time 10 min).

259
260 The hydrogen-isotopic composition of hydrocarbon and FAME fractions was
261 measured with continuous-flow GC - isotope ratio - MS. Purified extracts were
262 concentrated and injected (1-2 µl) into a Thermo Trace Ultra GC equipped with a
263 30m×250 µm HP5 (0.25 µm thick film) capillary GC column. Oven conditions were
264 similar to the setting used for the quantification. The conversion of organic
265 biomarkers to elemental hydrogen was accomplished by high-temperature
266 conversion (HTC) at 1420°C (Thermo GC Isolink). After the HTC, H₂ was introduced
267 into the isotope ratio MS (Thermo Scientific™ Delta V™IRMS) for compound-specific
268 determination of δ²H values via a Thermo ConFlo IV. Following a linearity test, we only
269 used peaks with amplitude (mass 2) between 1500 and 8000 mV for the evaluation.
270 The δ²H values were calibrated against saturated HMW *n*-alkanes using the reference

276 substance mix A4 (Biogeochemical Laboratories, Indiana University). The H_3^+ factor
277 ([Sessions et al., 2001](#)) was determined every day and stayed constant ($<3\text{‰}/V$)
278 throughout [our analyses period](#). Each purified extract was injected three times.
279 FAMES were further corrected to account for the methylation agent by comparing the
280 hydrogen abundance of lauric acid (C_{12} -FA; i.e. 12 carbon atoms) as acid and
281 corresponding methyl ester. The average methylation [correction](#) for lauric acid was
282 $23.97 \pm 3.9\text{‰}$ ($n=4$). This [correction](#) was, normalized to chain length (i.e. increasing
283 chain lengths result in lower corrections), applied to all the FAMES. δ^2H values of n -
284 alkanes and FAMES are reported as mean, standard deviation and weighted average,
285

Formatted: Subscript

Formatted: Superscript

Deleted: the evaluation

Deleted: effect

Deleted: factor

Deleted: (Table 5)

286 [Details of the analytical methods for extraction, work-up, and purification of the eight](#)
287 [offshore sediment samples for biomarker analysis that are included in our source-](#)
288 [apportionment comparison \(section 4.3\) can be found in Bröder et al. \(2016b\). The](#)
289 [\$\delta^2H\$ analysis on the shelf sediments was performed in parallel with the ICD-PF and](#)
290 [Topsoil-PF samples, according to the method described above.](#)
291

Formatted: Font:Symbol

Formatted: Superscript

292 2.3 Source apportionment

293 The compound-specific δ^2H signatures in this study were used to differentiate
294 between the two major sources (end-members), Topsoil-PF and ICD-PF, using an
295 isotopic mass-balance model. We used a Markov chain Monte Carlo (MCMC) approach
296 to account for the end-member variability (Andersson et al., 2015; Bosch et al., 2015).
297 The end-members were represented by normal distributions, with mean and
298 standard deviations obtained [from our analysis \(\$\delta^2H\$ on TS and ICD samples\) and](#)
299 [from literature \(\$\delta^{13}C\$ and \$\Delta^{14}C\$ on end-members\)](#). For each Laptev Sea station, the
300 isotope signatures from three different terrestrial molecular markers (long-chain n -
301 alkanes C_{27} , C_{29} and C_{31}) were used jointly to improve source apportionment
302 precision. The δ^2H signatures for the two end-members were based on our Topsoil-
303 PF and ICD-PF samples,
304

Formatted: Font:12 pt

Formatted: Font:Symbol, 12 pt

Formatted: Font:12 pt, Superscript

Formatted: Font:12 pt

Formatted: Font:Symbol, 12 pt

Formatted: Font:12 pt, Superscript

Formatted: Font:12 pt

Deleted: from the literature values

Formatted: Font:Symbol, 12 pt

Formatted: Font:12 pt, Superscript

Formatted: Font:12 pt

Deleted: (see Table 5 for mean source values)

305 The compound-specific δ^2H -based source apportionment was compared to
306 $\Delta^{14}C/\delta^{13}C$ -based analysis of bulk OC using analogous MCMC techniques (e.g., Vonk et
307 al., 2012). The $\Delta^{14}C/\delta^{13}C$ -approach allows estimation of the relative contribution of a
308 third source, marine, which does not affect the presently investigated (terrestrial)
309 compounds. Accounting for the marine component to OC allows direct comparison of
310 the Holocene and Pleistocene contributions. All MCMC calculations were made using
311 Matlab scripts (ver. 2014b) using 200,000 iterations, a burn-in phase (initial search
312 period) of 10,000 and a data thinning of 10.
313

314 The spatial extent of ICD in the Lena River Basin was calculated by overlaying
315 the extent of the drainage basin (from WRIBASIN: Watersheds of the World
316 published by the World Resources Institute, [www.wri.org/publication/watersheds-](http://www.wri.org/publication/watersheds-world)
317 [world](http://www.wri.org/publication/watersheds-world)) with the extent of the Yedoma Region (digitized from Romanovsky, 1993) in
318 an equal area map projection. It was assumed that 30% of the Yedoma Region consists
319 of intact ICD (following Strauss et al., 2013).
320

3 Results

3.1 Bulk geochemistry

The investigated Topsoil-PF and ICD-PF samples are, on a bulk geochemical level, very different. Mean organic carbon contents (as %OC) and total nitrogen content (as %TN) are 25 ± 12 and 1.1 ± 0.67 for Topsoil-PF samples, and 1.6 ± 0.31 and 0.17 ± 0.058 for ICD-PF samples, respectively (Table 1). This gives TOC/TN ratios of 25 ± 8.0 for Topsoil-PF samples and 10 ± 2.6 for ICD-PF samples. Stable carbon isotopic values of Topsoil-PF and ICD-PF samples are $-27.8 \pm 1.3\text{‰}$ and $-25.7 \pm 0.75\text{‰}$, respectively (Table 1). Radiocarbon ages were unfortunately only available for a few ICD samples, and ranged between 17 and 28 ¹⁴C ka (Table 1).

Formatted: Superscript

3.2 Molecular geochemical composition

Long-chain *n*-alkanes and *n*-alkanoic acids are abundant in epicuticular waxes and therefore indicative for a source of higher plants (Eglinton and Hamilton, 1967). Concentrations of individual long-chain *n*-alkanes in Topsoil-PF samples ranged from 1 to 340 $\mu\text{g/gOC}$ (C_{21} - C_{33} ; Table 2) with an average chain length of 28 ± 1.6 . The sum of high-molecular weight (HMW) *n*-alkanes ($>\text{C}_{21}$) for Topsoil-PF samples was 418^{612}_{280} $\mu\text{g/gOC}$ (median with interquartile range) and the most abundant *n*-alkanes added up to 214^{494}_{148} $\mu\text{g/gOC}$ (sum of C_{25} - C_{27} - C_{29} - C_{31}) (Table 4, Fig. 2a). For ICD-PF samples, the individual concentrations of long-chain *n*-alkanes were between 4 and 160 $\mu\text{g/gOC}$, and the average chain length 27 ± 0.7 (Table 2). The sum of high-molecular weight *n*-alkanes, and most abundant *n*-alkanes were 698^{806}_{630} $\mu\text{g/gOC}$ and 347^{405}_{323} $\mu\text{g/gOC}$, respectively (Table 4, Fig. 2a). The carbon preference index (CPI), a molecular ratio indicative for degradation status with values >5 typical for fresher terrestrial material and values approaching 1 typical for more degraded samples (Hedges and Prahl, 1993), showed values for Topsoil-PF samples of 7.3 ± 3.6 (average \pm standard deviation) and ICD-PF samples of 3.6 ± 0.8 (CPI C_{23} - C_{31} ; Table 4, Fig. 2c). The $\text{C}_{25}/(\text{C}_{25}+\text{C}_{29})$ ratio, indicative for the input of peat moss (*Sphagnum sp.*) material (Vonk and Gustafsson, 2009; *Sphagnum* values 0.72, higher plants 0.07; Nott et al., 2000) was 0.33 ± 0.22 (average \pm standard deviation) and 0.34 ± 0.05 for Topsoil-PF and ICD-PF samples, respectively (Table 4). Another commonly used *Sphagnum* proxy (Bush and McInerney, 2013), $\text{C}_{23}/(\text{C}_{23}+\text{C}_{29})$, resulted in a sharper contrast between ICD-PF and Topsoil-PF samples (0.39 ± 0.13 and 0.25 ± 0.23 , respectively; Fig. 2e and Table 4).

Deleted: 420 \pm 330

Deleted: \pm IQR;

Deleted: 210 \pm 350

Deleted: 700 \pm 180

Deleted: 350 \pm 81

Long-chain *n*-alkanoic acids (C_{22} and above) were abundant in concentrations between 0.122 and 2670 $\mu\text{g/gOC}$ for individual homologues in topsoils, with the sum of HMW *n*-alkanoic acids ($>\text{C}_{22}$) being 6397^{7454}_{3167} $\mu\text{g/gOC}$ (median and JQR) and the most abundant *n*-alkanoic acids (sum of C_{22} - C_{24} - C_{26} - C_{28}) adding up to 4700^{6092}_{2670} $\mu\text{g/gOC}$ (Table 3, 4 and Fig. 2b). ICD-PF samples contained individual long-chain *n*-alkanoic acids in 2.17 and 18700 $\mu\text{g/gOC}$ (Table 2), a sum of HMW *n*-alkanoic acids of 8290^{11430}_{6290} $\mu\text{g/gOC}$, and the sum of most abundant, even *n*-alkanoic acids of 6630^{8790}_{5285} $\mu\text{g/gOC}$ (Table 4). Topsoil-PF and ICD-PF samples had average chain lengths of 24.1 ± 1.1 and 24.3 ± 0.59 , and CPI (C_{22} - C_{28}) values of 5.9 ± 2.7 (average \pm standard

Formatted: Font:Italic

Formatted: Subscript

Formatted: Subscript

Formatted: Subscript

Deleted: .

Deleted: 6400 \pm 4300

Deleted: \pm

Deleted: 4700 \pm 3400

Deleted: 2

Deleted: 3

Deleted: 8300 \pm 5100

Deleted: 6600 \pm 3500

385 deviation) and 5.0 ± 1.6 , respectively (Table 4). Shorter-chain *n*-alkanoic acids C₁₆ and
386 C₁₈ are produced in basically all types of life in soils or aquatic environments, and are
387 not specific for higher plants. Topsoil-PF contained C₁₆ and C₁₈ homologues in
388 concentrations between 220 and 4600 $\mu\text{g/gOC}$, and ICD-PF samples between 200 and
389 10400 $\mu\text{g/gOC}$ (Table 3).

390

391 Degradation of organic matter involves the loss of functional groups, e.g. the loss of
392 carboxylic acids (Meyers and Ishiwatari, 1993). A high ratio of HMW *n*-alkanoic acids
393 over HMW *n*-alkanes in a sample therefore implies a relatively fresh, less degraded,
394 status (i.e. relatively more functional groups present). For Topsoil-PF samples, the
395 HMW *n*-alkanoic acid/HMW *n*-alkane ratio varied between 5.6 and 25 with an
396 average value of 13 ± 7.6 , whereas ICD-PF samples varied between 7.6 and 140 with
397 an average value of 29 ± 43 (Table 4, Fig. 2f).

398

399 3.3 Molecular isotopic composition

400 We measured $\delta^2\text{H}$ values in long-chain *n*-alkanes and *n*-alkanoic acids between -119
401 and -313‰ (Fig. 3, Table 5). Mean values for HMW *n*-alkanes (C₂₅-C₂₇-C₂₉-C₃₁) were
402 between -201 and -247‰ for Topsoil-PF samples and between -221 and -297‰ for
403 ICD-PF samples, with consistently lower $\delta^2\text{H}$ for longer chain lengths. For HMW *n*-
404 alkanolic acids (C₂₂-C₂₄-C₂₆-C₂₈) mean $\delta^2\text{H}$ values were between -203 and -236‰ for
405 Topsoil-PF samples and between -261 and -278‰ for ICD-PF samples (Table 5). The
406 decrease in $\delta^2\text{H}$ values with increasing chain length is less distinct for *n*-alkanoic acids
407 but one can observe a decrease of around 25-30‰ from C₂₂ to C₂₆ (Fig. 3). For ICD-
408 PF samples, the isotopic depletion for the average of the three most abundant *n*-
409 alkanes is comparable to the average for *n*-alkanoic acids, whereas in Topsoil-PF
410 samples, the isotopic depletion for the three most abundant *n*-alkanes is a bit larger
411 than for *n*-alkanoic acids (Fig. 4).

412

413 4 Discussion

414

415 4.1 Using bulk geochemistry and molecular proxies

416 Bulk geochemical and isotopic analysis, as well as analysis of molecular proxies
417 remained inconclusive in distinguishing between the two investigated sources in this
418 study. Topsoil-PF samples have a higher organic content, higher TOC/TN values
419 (representing fresh, higher plant material; Meyers, 1994) and more depleted $\delta^{13}\text{C}$
420 values (indicative for terrestrial C3 plants; Meyers, 1997) than ICD-PF samples,
421 suggesting that these samples indeed trace a fresh soil and/or vegetation source
422 (Table 1). The $\delta^{13}\text{C}$ values of a larger ICD-PF and Topsoil-PF dataset have earlier been
423 summarized (Vonk et al., 2012 and references therein; Schirrmeister et al., 2011)
424 giving values of $-26.3 \pm 0.67\text{‰}$ (n=374) and $-28.2 \pm 2.0\text{‰}$ (n=30), respectively. Our
425 values (Table 1) are in a similar range. Despite the differences between these two
426 sources in their bulk geochemistry, it is hard to use these parameters for source
427 distinction as their variability is fairly high, and their behavior in the environment is
428 not conservative, but e.g. affected by degradation processes. On a molecular
429 geochemical level the two investigated sources are virtually indistinguishable as

Deleted: it seems that

Deleted: h

432 there is a considerable variation in molecular concentrations and proxy values (Fig.
433 2). Only one of the tested parameters, the CPI C_{23} - C_{31} of *n*-alkanes, showed a
434 statistically significantly different value for the two investigated sources.
435

436 4.2 Evaluation of molecular δ^2H values as a source end-member

437 To alleviate the difficulty to distinguish between Topsoil-PF and ICD-PF with just bulk
438 and molecular geochemical characteristics, we explore the δ^2H values of leaf wax
439 molecules (i.e. long chain *n*-alkanoic acids and *n*-alkanes) to differentiate between
440 their relative source contributions. The overall mean δ^2H of the four most abundant
441 *n*-alkanoic acids is $-231\pm 29\text{‰}$ and $-271\pm 13\text{‰}$ for Topsoil-PF and ICD-PF samples,
442 respectively. These values compare well with available literature (Fig. 5). Pautler et
443 al. (2014) measured δ^2H values on C_{29} *n*-alkanes in modern soils of the Yukon, Canada
444 of $-252\pm 9.1\text{‰}$ ($n=4$) and aged soil δ^2H values of $-269\pm 8.6\text{‰}$ ($n=13$; 24-25 ^{14}C -ka ago)
445 and $-273\pm 16.4\text{‰}$ ($n=9$; for MIS 4, ~ 70 ^{14}C -ka ago). Yang et al. (2011) also reported
446 C_{29} *n*-alkane δ^2H values for modern vegetation from Alaska and Arctic Canada with an
447 average value of $-252\pm 43\text{‰}$ ($n=8$). Zech et al. (2011) reported values of C_{29} *n*-alkanes
448 collected from a permafrost exposure along the Tumara River in northeast Siberia,
449 with an average value of $-266\pm 7.5\text{‰}$ ($n=23$) for glacial paleosoils and $-247\pm 9.4\text{‰}$
450 ($n=17$) for interglacial paleosoils. Our values for C_{29} *n*-alkanes for Topsoil-PF ($-$
451 $246\pm 13\text{‰}$; $n=9$) and ICD-PF ($-280\pm 12\text{‰}$; $n=9$) are in a similar range (Fig. 5). For C_{28}
452 *n*-alkanoic acids, Wilkie et al. (2013) measured $-252\pm 8.7\text{‰}$ ($n=6$) for modern
453 vegetation in northeast Siberia, whereas Porter et al. (2016) measured $-269\pm 2.7\text{‰}$
454 ($n=7$) for ca. 31 cal ka BP old soils in the Yukon. Compared to these studies, our values
455 for C_{28} *n*-alkanoic acids are somewhat more enriched for Topsoil-PF with $-220\pm 15\text{‰}$
456 ($n=7$) but roughly in the same range for ICD-PF with $-267\pm 16\text{‰}$ ($n=9$).
457

458 The mean isotopic difference between the most abundant *n*-alkanoic acids of the two
459 investigated sources is around 40‰ (δ^2H values of $-231\pm 29\text{‰}$ and $-271\pm 13\text{‰}$ for
460 Topsoil-PF and ICD-PF samples, respectively). Despite the relatively large standard
461 deviations, the isotopic differences are statistically significant for each of the *n*-
462 alkanoic acids individually (C_{22} , C_{24} , C_{26} , C_{28} ; Fig. 3). The isotopic differences between
463 the two sources for the mean value of the four most abundant *n*-alkanes is 35‰ , with
464 a mean value of $-229\pm 33\text{‰}$ and $-264\pm 34\text{‰}$ for Topsoil-PF and ICD-PF samples,
465 respectively. Here, the individual *n*-alkane isotopic signatures are statistically
466 significantly different for C_{27} , C_{29} , C_{31} (Fig. 3) in Topsoil-PF and ICD-PF samples. The
467 selection and application of individual chain length δ^2H values as end-members, in
468 contrast to mean chain length values, might be more appropriate for several reasons;
469 (i) to reduce variability (δ^2H ranges for C_{29} and C_{31} *n*-alkanes and C_{22} and C_{24} *n*-
470 alkanoic acids are relatively low; Fig. 3), (ii) to target the most abundant species (C_{29}
471 and C_{31} *n*-alkanes are generally more abundant in soils and ICD-PF compared to
472 shorter chain lengths; Table 2), and (iii) to make use of the largest dynamic range
473 between source end-member values (C_{31} *n*-alkane δ^2H values of Topsoil-PF and ICD-
474 PF differ by 50‰). Based on these arguments, the C_{28} *n*-alkanoic acid and the C_{29} or
475 C_{31} *n*-alkanes are most appropriate to use for source-apportionment. The available

476 previous studies (Fig. 5) have also selected these chain lengths (C₂₈ *n*-alkanoic acid
477 and C₂₉ *n*-alkanes) for proxy development.

478
479 The use of molecular δ²H values as tracers of terrestrial material in a marine or
480 coastal setting has the advantage that it avoids uncertainty issues related to definition
481 of the marine end-member. On the other hand, the inherent bulk-upscaling challenge
482 of any molecular proxy, is a disadvantage of the δ²H approach as it introduces
483 unknowns related to the molecular-bulk upscaling effort (e.g. taking into account
484 sorting and recalcitrance; discussed in depth in 4.3). We also want to emphasize that
485 δ²H leaf wax values in the two studied end-member sets (Topsoil-PF vs. ICD-PF)
486 largely depend on the climate (warm vs. cold) and continentality (near the coast vs.
487 further inland) during plant formation, and associated differences in fractionation
488 mechanisms. Consequently, when δ²H values in samples are used for source-
489 apportionment, this may represent the fraction leaf wax produced in cold vs. warm
490 conditions (as well as degree of continentality), and not necessarily the fraction
491 Topsoil-PF vs. ICD-PF.

492
493 Finally, we realize that the amount of soil and ICD samples analyzed in this study is
494 limited, and want to point out that the results may change when more data are
495 analyzed in the near future. Additionally, studies have shown that the δ²H signature
496 of ice within ICD permafrost deposits can range from roughly -150‰ to -260‰
497 depending on the type of ice (wedge ice vs. pore or texture ice) as well as the period
498 of formation (different Pleistocene cold stages) (Opel et al., 2017 and references
499 therein). The source of water (i.e. type of ice) and age of the deposit will therefore
500 influence the *n*-alkane or *n*-alkanoic acid δ²H signal. However, regardless of the
501 natural variability associated with the processes mentioned above, both ICD and
502 texture-ice isotopic compositions appear to reflect long-term climate changes (Opel
503 et al., 2017; Schwamborn et al., 2006; Dereviagin et al., 2013; Porter et al., 2016)
504 which, likely, were also captured in the *n*-alkane or *n*-alkanoic acid δ²H signal.
505 Unfortunately, we do not have ¹⁴C-ages available for all ICD samples, so cross-
506 referencing to published stratigraphies in the region is not possible. Coastal
507 sediments, however, will represent a mixture of material released from different
508 depths, outcrops, and stratigraphies within the catchment or coast. For source-
509 apportionment applications, we reason that a growing body of leaf wax δ²H end-
510 member data from the ICD region can overcome the variability issues highlighted
511 above.

512 513 **4.3 Comparison with ¹³C-¹⁴C source-apportionment: a case-study**

514 Bulk OC dual-carbon isotope data provide a quantitative apportionment tool to assess
515 the relative contributions of Topsoil-PF vs. ICD-PF. Here, we present a case-study of
516 a shelf-slope transect in the Laptev Sea (Fig. 1) where both these source-
517 apportionment tools for the first time can be applied, compared and evaluated. The
518 shelf-slope transect of eight surface sediment samples stretches over 600 km from
519 the nearshore zone (72.7°N, <10m water depth) to the continental rise (78.9°N,

Deleted: ies

Formatted: Font: Cambria, Not Italic

Formatted: Font: +Theme Body (Cambria)

Formatted: Font: +Theme Body (Cambria), 12 pt, Not Italic

Formatted: Font: 12 pt

Formatted: Font: Italic

Formatted: Font: Italic

Formatted: Font: Symbol

Formatted: Superscript

Formatted: Font: +Theme Body (Cambria), 12 pt, Not Italic

Formatted: Font: +Theme Body (Cambria), 12 pt

Formatted: Font: +Theme Body (Cambria), 12 pt, Not Italic

Formatted: Font: +Theme Body (Cambria), 12 pt

Formatted: Font: +Theme Body (Cambria), 12 pt, Not Italic

Formatted: Font: Symbol, 12 pt, Not Italic

Formatted: Font: +Theme Body (Cambria), 12 pt, Not Italic, Superscript

Formatted: Font: +Theme Body (Cambria), 12 pt, Not Italic

Formatted: Superscript

Formatted: Font: Symbol

Formatted: Superscript

521 >3000m depth) (Table 6). More molecular and bulk geochemical characteristics of
522 these samples can be found in Bröder et al. (2016b).

523
524 The $\delta^{13}\text{C}-\Delta^{14}\text{C}$ source-apportionment uses three end-members (marine, Topsoil-PF,
525 and ICD-PF). End-member values are based on previously published values (Tesi et
526 al., 2016); with a $\delta^{13}\text{C}$ value of $-27.0\pm 1.2\text{‰}$ (n=38; Rodionow et al., 2006; Tesi et al.,
527 2014; Gundelwein et al., 2007; Bird et al., 2002) for Topsoil-PF, and $-26.3\pm 0.67\text{‰}$
528 (n=374; Vonk et al., 2012; Schirrmeister et al., 2011) for ICD-PF. The Topsoil-PF $\Delta^{14}\text{C}$
529 endmember was defined as $-232\pm 147\text{‰}$ (n=29; Winterfeld et al., 2015; Jasinski et al.,
530 1998; Kaiser et al., 2007; Höfle et al., 2013; Palmtag et al., 2015). For ICD-PF we used
531 a $\Delta^{14}\text{C}$ value of $-940\pm 84\text{‰}$ (n=300; Vonk et al., 2012 and references therein). The
532 marine end-member value was $-21.0\pm 2.6\text{‰}$ (n=10; Panova et al., 2015) and $-$
533 $50.4\pm 12\text{‰}$ (n=10; Panova et al., 2015) for $\delta^{13}\text{C}$ and $\Delta^{14}\text{C}$, respectively. Calculations
534 were made using a Markov chain Monte Carlo approach (see 2.3).

535
536 For $\delta^2\text{H}$ source-apportionment there is no need to include a marine end-member as
537 marine organisms do not produce long-chain *n*-alkanes or *n*-alkanoic acids. We were
538 unfortunately only able to analyze *n*-alkanes in the shelf-slope transect samples, and
539 no *n*-alkanoic acids, due to limitations in sample volume. We used the $\delta^2\text{H}$ values of
540 the C_{27} , C_{29} and C_{31} *n*-alkanes, individually. In other words, these three chain lengths
541 are taken as independent markers, providing an overdetermined system (i.e. two
542 sources defined with three different markers). This is more representative than using
543 the average (concentration-weighted) $\delta^2\text{H}$ value for these *n*-alkanes as the end-
544 member values for each chain length are different. For Topsoil-PF we used $-$
545 $215\pm 39\text{‰}$, $-246\pm 13\text{‰}$, and $-247\pm 23\text{‰}$ for C_{27} , C_{29} and C_{31} *n*-alkanes, and for ICD-PF
546 we applied $-259\pm 18\text{‰}$, $-297\pm 15\text{‰}$, and $-282\pm 13\text{‰}$ for C_{27} , C_{29} and C_{31} *n*-alkanes,
547 respectively (see also Table 5). Afterwards, we averaged the three end-member
548 contributions derived from the three calculations for each station, thereby taking the
549 variability introduced by the end-members into account.

550
551 The source apportionment of OC from Topsoil-PF and ICD-PF to surface sediments
552 along the Laptev Sea transect differ between the bulk $\delta^{13}\text{C}-\Delta^{14}\text{C}$ and leaf wax $\delta^2\text{H}$
553 approaches (Table 6). The former approach suggests Topsoil-PF contributions
554 between 21-70%, generally decreasing offshore, and, consequently, ICD-PF
555 contributions of 30-79%, generally increasing offshore. The latter (leaf wax $\delta^2\text{H}$)
556 approach results in a more extreme division of sources with Topsoil-PF contributions
557 of 83-91% and ICD-PF contributions of 9-17%, with similar patterns nearshore and
558 offshore (Table 6). A contribution of 9-17% may seem more in line with the estimated
559 extent of ICD in the Lena River basin: 12% of the basin falls within the Yedomia Region
560 (as defined by Romanovsky, 1993) and about 3% consists of intact ICD (see section
561 2.3). However, the cross-shelf sites are also strongly influenced by coastal and/or
562 subsea erosion (Karlsson et al. 2011; Vonk et al., 2012; Semiletov et al., 2012; 2016)
563 so the catchment characteristics are only one part of the story. It is challenging to
564 interpret the differences between the two proxies but we elaborate below on
565 potential reasons.

566
567 Assumptions in the bulk $\delta^{13}\text{C}$ - $\Delta^{14}\text{C}$ approach may affect these results. First, the
568 outcome of the bulk $\delta^{13}\text{C}$ - $\Delta^{14}\text{C}$ approach is sensitive to the definition of the marine
569 end-member. Changes in the currently used $\delta^{13}\text{C}$ and $\Delta^{14}\text{C}$ value of the marine end-
570 member of the East Siberian Arctic Shelf (n=10; Panova et al., 2015) would likely alter
571 the relative Topsoil-PF and ICD-PF contributions. The currently used standard
572 deviation for the $\delta^{13}\text{C}$ marine end-member is 2.6‰, which is much higher than the
573 values for the terrestrial end-members. Second, lateral transport time enroute the
574 shelf-slope transect (>600 kilometers) causing potentially significant aging of
575 sediments and its organic carbon is not accounted for in the source-apportionment.
576 Lateral transport time results in older surface OC ages on the shelf, compared to those
577 at the initial coastal deposition. Without correcting for this factor, the source-
578 apportionment will generate lower contributions of the (younger) Topsoil-PF
579 component. In an attempt to estimate this effect, we recalculated (similar to Bröder
580 et al. 2016a) the relative source contributions of Topsoil-PF, ICD-PF (and marine)
581 with the bulk $\delta^{13}\text{C}$ - $\Delta^{14}\text{C}$ approach with the assumption that the Topsoil-PF ^{14}C age
582 would be subject to a cross-shelf lateral transport time of 5000 yrs. We assumed a
583 linear aging along the transect based on distance from the coast, with a maximum
584 value of 5000 yrs aging at station SW-01. This resulted in Topsoil-PF contributions
585 that were up to 20% higher (for the deepest stations) compared to the source-
586 apportionment where lateral transport time was unaccounted for (Table 6; Fig. 6).
587

588 Assumptions in the leaf wax $\delta^2\text{H}$ source-apportionment approach could potentially
589 also impact the outcomes, and hence differences with the bulk $\delta^{13}\text{C}$ - $\Delta^{14}\text{C}$ results. First,
590 there is an inherent assumption related to the molecular to bulk level upscaling
591 challenge. We assume that the physical association of *n*-alkanes in different source
592 end-members (Topsoil-PF vs. ICD-PF) as well as their fractionation in the coastal
593 system is similar. However, previous research has shown that *n*-alkanes behave
594 rather differently upon their release into coastal waters; *n*-alkanes originating from
595 surface soil or vegetation debris are not bound to minerals and remain in suspension
596 during transport while being actively degraded, whereas *n*-alkanes originating in
597 deeper mineral soils settle quickly and are protected from extensive degradation
598 (Vonk et al., 2010). It is possible that most of the *n*-alkanes in the Laptev Sea sediment
599 transect originate in (deeper) mineral soils. An effect of physical association, as well
600 as the potential effect of hydrodynamic sorting patterns (Tesi et al., 2016) on the leaf
601 wax $\delta^2\text{H}$ values of both sources could impact the source-apportionment. Another
602 factor that can introduce a bias in our leaf wax $\delta^2\text{H}$ approach is a proton exchange of
603 the C-bound H-atoms in *n*-alkanes with environmental water, either from in situ
604 sources (soil water) or during transport (river or ocean water, or sediment pore
605 water). As there is no evidence for such exchange in young (<1 million years), cold
606 sediments (Sessions et al., 2004) we suspect this process may be minimal in our
607 samples (and end-members).
608

609 When accounting for an estimated lateral transport time, the difference in estimates
610 of source contribution by the two different approaches (bulk $\delta^{13}\text{C}$ - $\Delta^{14}\text{C}$ and leaf wax

Deleted: Although t

Deleted: this process could be enhanced in environments of low pH. The precise effect of such exchange on the $\delta^2\text{H}$ signal of our samples (or end-members) is unknown, but we

616 $\delta^2\text{H}$) increases offshore, from about a 25% difference near the coast to a 40%
617 difference at stations SW-01 and SW-03. This increasing offset between the results of
618 the two end-member mixing methods may be caused by several factors such as
619 variability in the marine end-member (e.g. due to changes in seasonal ice cover), a
620 selective degradation (of the topsoil OC) enroute that introduces a source bias or
621 isotopic fractionation, or remaining factors related to the lateral transport time
622 (incorrect assumption of 5000 years, non-linear aging along transect). These
623 differences highlight that both source-apportionment tools still could be fine-tuned
624 further by (i) increasing the sample size of sources to reduce end-member
625 uncertainties, (ii) continuous adjustments in end-member values and Markov chain
626 Monte Carlo calculations based on latest knowledge, and (iii) assuring regional
627 testing and verification of the method when applied to new environments.

628

629 5 Conclusions

630 Leaf wax $\delta^2\text{H}$ values in samples from aquatic recipient environments can be used to
631 source-apportion the incoming terrestrial OC into two end-members; a Pleistocene
632 ICD permafrost source and a younger, Holocene, topsoil source. Mean isotopic values
633 of the C_{29} *n*-alkane, C_{31} *n*-alkane, and C_{28} *n*-alkanoic acid showed a dynamic,
634 statistically significant range of 34, 50 and 46‰ between Topsoil-PF and ICD-PF
635 samples, respectively, with ICD-PF samples being consistently more depleted
636 indicative of formation during the colder and drier Pleistocene.

637

638 A case-study where we tested two isotopic proxies (leaf wax $\delta^2\text{H}$ and bulk $\delta^{13}\text{C}-\Delta^{14}\text{C}$)
639 to calculate the relative terrestrial source contribution of Topsoil-PF and ICD-PF
640 along a Laptev Sea surface sediment transect, showed that the two proxies yield
641 variable results but overall generate similar trends offshore. We reason that
642 variability is caused by factors such as lateral transport time, remaining uncertainties
643 in end-member definition, or environmental factors such as physical association.

644

645 Both methods (leaf wax $\delta^2\text{H}$ and bulk $\delta^{13}\text{C}-\Delta^{14}\text{C}$) bring along their inherent
646 disadvantages and advantages. The molecular approach has the distinct advantage
647 that it circumvents the uncertainties that are associated with marine end-member
648 definition in the case of bulk OC mixing model analysis. However, application of
649 molecular $\delta^2\text{H}$ in source-apportionment studies brings along challenges related to the
650 molecular-bulk upscaling step. Bulk $\delta^{13}\text{C}-\Delta^{14}\text{C}$ source-apportionment, on the other
651 hand, has the advantage to operate on a bulk and perhaps more representative level,
652 but is hampered by remaining uncertainties associated with the marine end-member.

653

654 This study shows that $\delta^2\text{H}$ of leaf wax molecules has the potential to be used in
655 quantitative source-apportionment studies of thawing permafrost in coastal or
656 marine settings. It can serve as an alternative or complementary approach to the
657 commonly applied bulk $\delta^{13}\text{C}-\Delta^{14}\text{C}$ method. We recommend continuing data collection
658 and optimization of end-member definition and calibration. Refining the molecular
659 $\delta^2\text{H}$ proxy presented here will be beneficial in pinpointing the location and extent of
660 OC release from thawing permafrost in the coastal or fluvial environment. With

Formatted: Font:Symbol

Formatted: Superscript

Deleted: in order to increase our understanding of the fate of

663 [enhanced Arctic warming and associated intensification of permafrost thaw,](#)
664 [constraining the amount and fate of permafrost OC release will help to assess the](#)
665 [magnitude of the permafrost carbon feedback to climate warming.](#)

667 **Data availability**

668 All data are available in Tables 1 through 6, as well as Supplementary Table S1.

670 **Acknowledgements**

671 We would like to acknowledge Robert Spencer, Sergey Davydov, Anya Davydova,
672 Ekatarina Bulygina, Peter Kuhry, Matthias Siewert, Juri Palmtag, Niels Weiss, Martin
673 Kruså, Volker Brüchert, Pete Hill, Vladimir Mordukhovich, Alexander Charkin, Deniz
674 Kosmach, Per Andersson, and sampling crew and personnel of IB Oden and RV Yakob
675 Smirnitskiy for help with sample collection in the field. Financial support has been
676 provided by the Dutch NWO (Veni #863.12.004), US-NSF (Polaris Project #1044610),
677 the Bolin Centre for Climate Research, the Knut and Alice Wallenberg Foundation
678 (SWERUS-C3 Program; KAW #2011.0027), the Swedish Research Council (VR #621-
679 2004-4039 and 621-2007-4631), the Russian Science Foundation (#15-17-20032 to
680 O. D.), the Nordic Council of Ministers Cryosphere-Climate-Carbon Initiative (project
681 Defrost, #23001), the European Research Council (ERCAdG project CC-TOP #695331
682 to Ö.G.). This study was supported by the Delta Facility of the Faculty of Science,
683 Stockholm University. GH would like to acknowledge funding from ESF-CryoCarb and
684 EU FP7-PAGE21 projects for topsoil and ICD sample collection. [The ISMAR](#)
685 [publication ID is #1931.](#)

Deleted: the Russian Government (mega-grant under contract #14.Z50.31.0012 to I. S.),

Formatted: Not Highlight

687 **Author contributions**

688 Land-based samples were collected by GH and JEV, ship-based samples were
689 collected by IS, OD, ÖG, TT, LB, and JEV. Laboratory analysis was performed by LB, TT,
690 and HH. Markov chain Monte Carlo simulations were run by AA. The manuscript was
691 written by JEV with input of all co-authors.

693 **References**

- 694 Anderson, L. G., Jutterström, S., Hjalmarsson, S., Wählström, I., and Semiletov, I.P.:
695 Out-gassing of CO₂ from Siberian Shelf seas by terrestrial organic matter
696 decomposition, *Geophys. Res. Lett.* 36, L20601, doi:10.1029/2009GL040046,
697 2009.
- 698 Anderson, L.G., Björk, G., Jutterström, S., Pipko, I., Shakhova, N. Semiletov, I. and
699 Wählström, I.: East Siberian Sea, an Arctic region of very high biogeochemical
700 activity, *Biogeosciences*, 8, 1745-1754, doi:10.5194/bg-8-1745-2011, 2011.
- 701 Andersson, E., Deng, J., Du, K., Zheng, M., Yan, C., Sköld, M., and Gustafsson, Ö.:
702 Regionally-varying combustion sources of the January 2013 severe haze events
703 over Eastern China, *Environ. Sci. Technol.* 49(4), 2038-2043, doi:
704 10.1021/es503855e, [2015.](#)
- 705 Bird, M. I., Santruckova, H., Arneith, A., Grigoriev, S., Gleixner, G., Kalaschnikov, Y. N.,
706 Lloyd, J., and Schulze, E.-D.: Soil carbon inventories and carbon-13 on a latitude
707 transect in Siberia, *Tellus*, 54B, 631-641, 2002.

Deleted: .

711 Bröder, L., Tesi, T., Salvado, J.A., Semiletov, I.P., Dudarev, O.V., and Gustafsson, Ö.:
712 Fate of terrigenous organic matter across the Laptev Sea from the mouth of the
713 Lena River to the deep sea of the Arctic interior, *Biogeosciences* 13, 5003, 5019,
714 doi:10.5194/bg-13-5003-2016, 2016b.

715 Bröder, L., Tesi, T., Andersson, A., Eglinton, T.I., Semiletov, I.P., Dudarev, O.V., Roos,
716 P., and Gustafsson, Ö.: Historical records of organic matter supply and
717 degradation status in the East Siberian Sea, *Org. Geochem.* 91, 16-30,
718 doi:10.1016/j.orggeochem.2015.10.008, 2016a.

719 Bosch, C., Andersson, A., Kruså, M., Bandh, C., Hovorkova, I., Klanova, J., Knowles, T.
720 D. J., Pancost, R. D., Evershed, R. P., and Gustafsson, Ö.: Source apportionment of
721 polycyclic aromatic hydrocarbons in central European soils with compound-
722 specific triple isotopes ($\delta^{13}\text{C}$, $\Delta^{14}\text{C}$, and $\delta^2\text{H}$), *Environ. Sci. Technol.* 49(13), 7657-
723 7665, doi:10.1021/acs.est.5b01190, 2015.

724 Bush, R.T., and McInerney, F.A.: Leaf wax n-alkane distributions in and across
725 modern plants: Implications for paleoecology and chemotaxonomy, *Geochim.*
726 *Cosmochim. Ac.* 117, 161-179, 2013.

727 Craig, H.: Isotopic variations in meteoric waters, *Science* 133: 1702-1703, 1961.
728 Dansgaard, W.: Stable isotopes in precipitation, *Tellus*, 16, 436- 438, 1964.

729 Eglinton, G., and Hamilton, R.J.: Leaf epicuticular waxes, *Science* 156, 1322-1335,
730 1967.

731 Gundelwein, A., Mueller-Lupp, T., Sommerkorn, M., Haupt, E. T. K., Pfeiffer, E. M., and
732 Wiechmann, H.: Carbon in tundra soils in the Lake Labaz region of arctic Siberia,
733 *Eur. J. Soil Sci.*, 58, 1164-1174, 2007.

734 Günther, F., Overduin, P.P., Sandakov, A.V., Grosse, G., and Grigoriev, M.N.: Short- and
735 long-term thermo-erosion of ice-rich permafrost coasts in the Laptev Sea region,
736 *Biogeosciences*, 10, 4297-4318, doi:10.5194/bg-10-4297-2013, 2013.

737 Hedges, J.I., and Prahl, F.G.: Early diagenesis: consequences for applications of
738 molecular biomarkers, in *Organic Geochemistry: principles and applications*. Engel,
739 M.H., and Macko, S.A. (ed.). Plenum Press, New York. pp 237-253, 1993.

740 Höfle, S., Rethemeyer, J., Mueller, C. W., and John, C.: Organic matter composition and
741 stabilization in a polygonal tundra soil of the Lena Delta, *Biogeosciences*, 10, 3145-
742 3158, doi:10.5194/bg-10-3145-2013, 2013

743 Hugelius, G. Strauss, J., Zubrzycki, S., Harden, J. W., Schuur, E. A. G., Ping, C.-L.,
744 Schirrmeister, L., Grosse, G., Michaelson, G. J., Koven, C. D., O'Donnell, J. A., Elberling,
745 B., Mishra, U., Camill, P., Yu, Z., Palmtag, J., and Kuhry, P.: Estimated stocks of
746 circumpolar permafrost carbon with quantified uncertainty ranges and identified
747 data gaps, *Biogeosciences* 11, 6573-6593, doi:10.5194/bg-11-6573-2014, 2014.

748 Jasinski, J. P. P., Warner, B. G., Andreev, A. A., Aravena, R., Gilbert, S. E., Zeeb, B. A., Smol,
749 J. P., and Velichko, A. A.: Holocene environmental history of a peatland in the Lena
750 River valley, Siberia, *Can. J. Earth Sci.*, 35, 637-648, 1998.

751 Johnsen, S. J., Dahl-Jensen, D., Gundestrup, N., Steffensen, J. P., Clausen, H. B., Miller,
752 H.: Oxygen isotope and palaeotemperature records from six Greenland ice-core
753 stations: Camp Century, Dye-3, GRIP, GISP2, Renland and NorthGRIP, *J. Quat. Sci.*
754 16, 299-307, doi:10.1002/jqs.622, 2001.

755 Kaiser, C., Meyer, H., Biasi, C., Rusalimova, O., Barsukov, P., and Richter, A.:
756 Conservation of soil organic matter through cryoturbation in arctic soils in

Deleted: .
Formatted: Font:12 pt, Not Italic
Formatted: Font:12 pt, Not Italic
Formatted: Font:12 pt, Not Italic
Formatted: Font:12 pt, Not Italic
Formatted: p1, Indent: Left: 0 cm, First line: 0 cm, Add space between paragraphs of the same style, Widow/Orphan control, Adjust space between Latin and Asian text, Adjust space between Asian text and numbers
Formatted: Font:+Theme Body (Cambria), 12 pt
Formatted: Font:+Theme Body (Cambria)
Deleted: .

- 759 Siberia, *J. Geophys. Res.-Biogeosciences*, 112, G2, doi:10.1029/2006JG000258,
760 2007.
- 761 Karlsson, E. S., Charkin, A., Dudarev, O., Semiletov, I., Vonk, J. E., Sanchez-Garcia, L.,
762 Andersson, A., and Gustafsson, O.: Carbon isotopes and lipid biomarker
763 investigation of sources, transport and degradation of terrestrial organic matter
764 in the Buor-Khaya Bay, SE Laptev Sea, *Biogeosciences* 8, 1865-1879,
765 doi:10.5194/bg-8-1865-2011, 2011.
- 766 Karlsson, E. S., Gelting, J., Tesi, T., van Dongen, B., Andersson, A., Semiletov, I.,
767 Charkin, A., Dudarev, O., and Gustafsson, Ö.: Different sources and degradation
768 state of dissolved, particulate, and sedimentary organic matter along the Eurasian
769 Arctic coastal margin, *Global Biogeochem. Cycles*, 30, 898-919,
770 doi:10.1002/2015GB005307, 2016.
- 771 Kotler, E., and Burn, C. R.: Cryostratigraphy of the Klondike "muck" deposits,
772 westcentral Yukon Territory, *Can. J. Earth Sci.* 37, 849-861, doi:10.1139/e00-013,
773 2000.
- 774 Leaney, F. W., Osmond, C. B., Allison, G. B., and Ziegler, H.: Hydrogen-isotope
775 composition of leaf water in C-3 and C-4 plants - its relationship to the hydrogen
776 isotope composition of dry-matter, *Planta* 164 (2), 215-220, 1985.
- 777 Meyer, H., Opel, T., Laepple, T., Dereviagin, A.Y., Hoffmann, K., and Werner, M.: Long-
778 term winter warming trend in the Siberian Arctic during the mid- to late
779 Holocene, *Nat. Geosci.* 8, 122-125, doi:10.1038/ngeo2349, 2015.
- 780 Meyers P. A., Ishiwatari R.: Lacustrine organic geochemistry – an overview of
781 indicators of organic matter sources and diagenesis in lake sediments, *Org.*
782 *Geochem.* 20, 867-900, doi:10.1016/0146-6380(93)90100-P, 1993.
- 783 Meyers, P. A.: Preservation of elemental and isotopic source identification of
784 sedimentary organic matter, *Chem. Geol.* 114, 289-302, doi:10.1016/0009-
785 2541(94)90059-0, 1994.
- 786 Meyers, P. A.: Organic geochemical proxies of paleoceanographic, paleolimnologic
787 and paleoclimatic processes, *Org. Geochem.* 27, 213-250, doi:10.1016/S0146-
788 6380(97)00049-1, 1997.
- 789 Nott, C. J., Xie, S., Avsejs, L. A., Maddy, D., Chambers, F. M., Evershed, R. P.: *n*-Alkane
790 distributions in ombrotrophic mires as indicators of vegetation change related to
791 climatic variation, *Org. Geochem.* 31, 231-235, doi:10.1016/S0146-
792 6380(99)00153-9, 2000.
- 793 Opel, T., Dereviagin, A. Y., Meyer, H., Schirrmeister, L., and Wetterich, S.:
794 Palaeoclimatic information from stable water isotopes of Holocene ice wedges on
795 the Dmitrii Laptev Strait, Northeast Siberia, Russia, *Permafrost Periglacial*
796 *Process.*, 22, 84-100, 10.1002/ppp.667, 2011.
- 797 Opel, T., Wetterich, S., Meyer, H., Dereviagin, A.Y., Fuchs, M.C., and Schirrmeister, L.:
798 Ground-ice stable isotopes and cryostratigraphy reflect late Quaternary
799 palaeoclimate in the Northeast Siberian Arctic (Oyogos Yar coast, Dmitry Laptev
800 Strait), *Clim. Past Discuss.*, doi:10.5194/cp-2017-1, 2017.
- 801 Palmtag J., Hugelius G., Lashchinskiy N., Tamstorf M.P., Richter A., Elberling B. and
802 Kuhry, P.: Storage, Landscape Distribution, and Burial History of Soil Organic
803 Matter in Contrasting Areas of Continuous Permafrost, Arctic, Antarctic, and Alpine
804 Research, 47(1), 71-88, doi: http://dx.doi.org/10.1657/AAAR0014-027, 2015.

Deleted: .

Deleted: .

Deleted: .

Formatted: Font:(Default) Times New Roman

Deleted: (2015)

809 Polissar, P. J., and Freeman, K. H.: Effects of aridity and vegetation on plant-wax dD in
810 modern lake sediments, *Geochim. Cosmochim. Ac.* 74, 5785-5797,
811 doi:10.1016/j.gca.2010.06.018, 2010.

812 Panova, E., Tesi, T., Pearce, C., Salvado, J. A., Karlsson, E. S., Kruså, M., Semiletov, I. P.,
813 and Ö. Gustafsson: Geochemical compositional differences of the supramicron
814 plankton-dominated fraction in two regimes of the Marginal Ice Zone (MIZ) of the
815 outer East Siberian Arctic Shelf, AGU Fall meeting 2015 abstract, 2015.

816 Pautler, B. G., Reichart, G.-J., Sanborn, P. T., Simpson, M. J., Weijers, J. W. H.:
817 Comparison of soil derived tetraether membrane lipid distributions and plantwax
818 dD compositions for reconstruction of Canadian Arctic temperatures,
819 *Palaeogeogr. Palaeoclimatol. Palaeoecol.* 404, 78-88,
820 doi:10.1016/j.palaeo.2014.03.038, 2014

821 Porter, T. J., Froese, D. G., Feakins, S. J., Bindeman, I. N., Mahoney, M. E., Pautler, B. G.,
822 Reichart, G.-J., Sanborn, P. T., Simpson, M. J., and Weijers, J. W. H.: Multiple water
823 isotope proxy reconstruction of extremely low last glacial temperatures in
824 Eastern Beringia (Western Arctic), *Quat. Sci. Rev.* 137, 113-125,
825 doi:10.1016/j.quascirev.2016.02.006, 2016.

826 Rodionow, A., Flessa, H., Kazansky, O., and Guggenberger, G.: Organic matter
827 composition and potential trace gas production of permafrost soils in the forest
828 tundra in northern Siberia, *Geoderma*, 135, 49-62, 2006.

829 Romanovsky, N. N.: Fundamentals of the cryogenesis of the lithosphere. University
830 Press, Moscow, pp. 1-336 (in Russian), 1993.

831 Sachse, D., Radke, J., and Gleixner, G.: Hydrogen isotope ratios of recent lacustrine
832 sedimentary n-alkanes record modern climate variability, *Geochim. Cosmochim.*
833 *Ac.*, 68, 4877-4889, doi:10.1016/j.gca.2004.06.004, 2004.

834 Schuur, E. A. G., McGuire, A. D., Schädel, C., Grosse, G., Harden, J. W., Hayes, D. J.,
835 Hugelius, G., Koven, C. D., Kuhry, P., Lawrence, D. M., Natali, S. M., Olefeldt, D.,
836 Romanovsky, V. E., Schaefer, K., Turetsky, M. R., Treat, C. C., and Vonk, J. E.:
837 Climate change and the permafrost carbon feedback, *Nature*, 250, 171-178,
838 doi:10.1038/nature14338, 2015.

839 Schirrmeister, L., Kunitzky, V. V., Grosse, G., Wetterich, S., Meyer, H., Schwamborn, G.,
840 Babiy, O., Derevyagin, A., and Siegert, C.: Sedimentary characteristics and origin of
841 the Late Pleistocene Ice Complex on north-east Siberian Arctic coastal lowlands
842 and islands – A review, *Quatern. Int.* 241, 3-25, doi:10.1016/j.quaint.2010.04.004,
843 2011.

844 Semiletov I.P., Pipko I.I., Shakhova N.E., Dudarev O.V., Pugach S.P., Charkin A.N., McRoy
845 C.P., Kosmach D., and Gustafsson, Ö: Carbon transport by the Lena River from its
846 headwaters to the Arctic Ocean, with emphasis on fluvial input of terrestrial
847 particulate organic carbon vs. carbon transport by coastal erosion, *Biogeosciences*,
848 8, 2407-2426, 2011.

849 Semiletov I.P., Shakhova N. E., Sergienko V.I., Pipko I.I., and O. Dudarev: On Carbon
850 Transport and Fate in the East Siberian Arctic Land-Shelf-Atmosphere System,
851 *Environment Res. Lett.*, 7, doi:10.1088/1748-9326/7/1/015201, 2012.

852 Semiletov, I.P., Shakhova, N.E., Pipko, I.I., Pugach, S.P., Charkin, A.N., Dudarev, O.V.,
853 Kosmach, D.A., and S. Nishino (2013). Space-time dynamics of carbon and

Deleted: t

855 environmental parameters related to carbon dioxide emissions in the Buor-Khaya
856 Bay of the Laptev Sea, *Biogeosciences*, 10, 5977-5996, doi:10.5194/bg-10-5977-
857 2013

858 Semiletov I., Pipko I., Gustafsson O., Anderson L., Sergienko V., Pugach S., Dudarev O.,
859 Charkin A., Broder L., Andersson A., Spivak E., and N. Shakhova (2016),
860 Acidification of the East Siberian Arctic Shelf waters through addition of
861 freshwater and terrestrial carbon, *Nature Geoscience*, doi:10.1038/NEGO 2695,
862 2016.

863 Semiletov I.P., Pipko, I.I., Pivovarov, N.Y., Popov, V. V., Zimov, S. A., Voropaev, Y. V.,
864 and S.P. Davydov: Atmospheric carbon emissions from northern lakes: a factor of
865 global significance, *Atmospheric Environment*, 30, 1657-1671, 1996a.

866 Semiletov I.P., Pivovarov, N.Y., Pipko, I. I., Gukov, A. Y., Volkova, T. I., Sharp, J. P.,
867 Shcherbakov, Y. S., and K. P. Fedorov: Dynamics of dissolved CH₄ and CO₂ in the
868 Lena River Delta and Laptev Sea. *Transactions (Doklady) of the Russian Academy
869 of Sciences*, 350 (3), 401-404 (translated into English), 1996b.

870 Semiletov, I.P.: Destruction of the coastal permafrost ground as an important factor
871 in biogeochemistry of the Arctic Shelf waters, *Trans. (Doklady) Russian Acad. Sci.*,
872 368, 679-682 (translated into English), 1999.

873 Sessions, A.L., Burgoyne, T.W., and Hayes, J.M.: Determination of the H3 factor in
874 hydrogen isotope ratio mass spectrometry, *Anal. Chem.* 73(2), 200-207, 2001.

875 Siewert, M.B., Hanisch, J., Weiss, N., Kuhry, P., Maximov, T.C., Hugelius, G.: Comparing
876 carbon storage of Siberian tundra and taiga permafrost ecosystems at very high
877 spatial resolution. *J. Geophys. Res.: Biogeosciences*, 120,
878 doi:10.1002/2015JG002999, 2015.

879 Siewert, M.B., Hugelius, G., Heim, B., Faucherre, S.: Landscape controls and vertical
880 variability of soil organic carbon storage in permafrost-affected soils of the Lena
881 River Delta. *Catena*, 147, 725-741. doi:10.1016/j.catena.2016.07.048, 2016.

882 Soil Survey Staff. *Keys to Soil Taxonomy*, 12th ed., U.S. Department of Agriculture &
883 Natural Resources Conservation Service, Washington, D. C., 2014.

884 Sessions, A. L., Burgoyne, T.W., Schimmelmann, A., and Hayes, J. M.: Fractionation of
885 hydrogen isotopes in lipid biosynthesis, *Org. Geochem.*, 30, 1193-1200,
886 doi:10.1016/S0146-6380(99)00094-7, 1999.

887 Sessions, A.L., Sylva, S.P., Summons, R.E., and Hayers, J.M.: Isotopic exchange of
888 carbon-bound hydrogen over geologic timescales, *Geochim. Cosmochim. Ac.* 68,
889 1545-1559, doi:10.1016/j.gca.2003.06.004, 2004.

890 Shakhova, N. and I. Semiletov: Methane release and coastal environment in the East
891 Siberian Arctic shelf, *Journal of Marine Systems*, 66 (1-4), 227-243, 2007.

892 Shakhova, N., Semiletov I., Leifer, I., , Sergienko, V., Salyuk, A., Kosmach, D., Chernikh
893 D., Stubbs Ch., Nicolsky D., Tumskoy V., and O. Gustafsson: Ebullition and storm-
894 induced methane release from the East Siberian Arctic Shelf, *Nature Geoscience*
895 7-1, 64-70, doi: 10.1038/NGEO2007, 2014.

896 Shakhova N., I. Semiletov, V. Sergienko, L. Lobkovsky, V. Yusupov, A. Salyuk, A.
897 Salomatin, D. Chernykh, D. Kosmach, G. Panteleev, D. Nicolsky, V. Samarkin, S.
898 Joye, A. Charkin, O. Dudarev, A. Meluzov, and Ö. Gustafsson: The East Siberian
899 Arctic Shelf: towards further assessment of permafrost-related methane fluxes and

Deleted: ournal of

Deleted: ical

Deleted: earch

Deleted: (2014),

Deleted: .

905 role of sea ice. *Phil. Trans. R. Soc. A*, vol. 373: 20140451.
906 doi:10.1098/rsta.2014.0451, 2015.

907 Shanahan, T.M., Hughen, K.A., Ampel, L., Sauer, P.E., and Fornace, K.: Environmental
908 controls on the 2H/1H values of terrestrial leaf waxes in the eastern Canadian
909 Arctic, *Geochim. Cosmochim. Ac.* 119, 286-301, doi:10.1016/j.gca.2013.05.032,
910 2013.

911 Shiklomanov, N. I., Streletskiy, D. A., Little, J. D., and Nelson, F. E.: Isotropic thaw
912 subsidence in undisturbed permafrost landscapes, *Geophys. Res. Lett.* 40, 6356-
913 6361, doi:10.1002/2013GL058295, 2013.

914 Smith, F.A., and Freeman, K.H.: Influence of physiology and climate on dD of leaf wax
915 n-alkanes from C3 and C4 grasses, *Geochim. Cosmochim. Ac.* 70, 1172-1187,
916 doi:10.1016/j.gca.2005.11.006, 2006.

917 Strauss, J., Schirrmeister, L., Grosse, G., Wetterich, S., Ulrich, M., Herzschuh, U., and
918 Hubberten, H.-W.: The deep permafrost carbon pool of the Yedoma region in
919 Siberia and Alaska. *Geophys. Res. Lett.* 40, 6165-6170,
920 doi:10.1002/2013GL058088, 2013.

921 Tesi, T., I. Semiletov, G. Hugelius, O. Dudarev, P. Kuhry, and Gustafsson, Ö.:
922 Composition and fate of terrigenous organic matter along the Arctic land-ocean
923 continuum in East Siberia: insights from biomarkers and carbon isotopes,
924 *Geochim. Cosmochim. Acta*, 133, 235-256, 2014.

925 Tesi, T., Semiletov, I., Dudarev, O., Andersson, A., and Gustafsson, Ö.: Matrix
926 association effects on hydrodynamic sorting and degradation of terrestrial organic
927 matter during cross-shelf transport in the Laptev and East Siberian shelf seas, *J.*
928 *Geophys. Res.-Biogeosciences*, 121, 731-752, doi:10.1002/2015JG003067, 2016a.

929 Tesi, T., Muschitiello, F., Smittenberg, R. H., Jakobsson, M., Vonk, J. E., Hill, P.,
930 Andersson, A., Kirchner, N., Noormets, R., Dudarev, O., Semiletov, I., and Gustafsson,
931 Ö.: Massive remobilization of permafrost carbon during post-glacial warming, in
932 review at *Nature Communications*, 2016b.

933 Vonk, J. E., van Dongen, B. E., and Gustafsson, Ö.: Selective preservation of old organic
934 carbon fluvially released from sub-arctic soils, *Geophys. Res. Lett.* 37, L11605,
935 2010

936 Vonk, J. E., Sánchez-García, L., van Dongen, B. E., Alling, V., Kosmach, D., Charkin, A.,
937 Semiletov, I. P., Dudarev, O. V., Shakhova, N., Roos, P., Eglinton, T. I., Andersson, A.,
938 and Gustafsson, Ö.: Activation of old carbon by erosion of coastal and subsea
939 permafrost in Arctic Siberia, *Nature*, 489, 137-140, doi:10.1038/nature11392,
940 2012.

941 Vonk, J. E., and Gustafsson, Ö.: Permafrost-carbon complexities, *Nat. Geosci.* 6, 675-
942 676, doi:10.1038/ngeo1937, 2013.

943 Vonk, J. E., Mann, P. J., Davydov, S., Davydova, A., Spencer, R. G. M., Schade, J.,
944 Sobczak, W. V., Zimov, N., Zimov, S., Bulygina, E., Eglinton, T. I., and Holmes, R. M.:
945 High biolability of ancient permafrost carbon upon thaw, *Geophys. Res. Lett.*, 40,
946 2689-2693, doi:10.1002/grl.50348, 2013.

947 Vonk, J. E., Semiletov, I. P., Dudarev, O. V., Eglinton, T. I., Andersson, A., Shakhova, N.,
948 Charkin, A., Heim, B., and Gustafsson, Ö.: Preferential burial of permafrost-derived
949 organic carbon in Siberian-Arctic shelf waters, *J. Geophys. Res. Oceans* 119, 8410-
950 8421, doi:10.1002/2014JC010261, 2014.

951 Vonk, J. E., Tank, S. E., Bowden, W. B., Laurion, I., Vincent, W. F., Alekseychik, P., Amyot,
 952 M., Billet, M. F., Canario, J., Cory, R. M., Deshpande, B. N., Helbig, M., Jammet, M.,
 953 Karlsson, J., Larouche, J., MacMillan, G., Rautio, M., Walter Anthony, K. M., and
 954 Wickland, K. P.: Effects of permafrost thaw on Arctic aquatic ecosystems,
 955 Biogeosciences 12, 7129-7167, doi:10.5194/bg-12-7129-2015, 2015.

956 Walvoord, M. A., Voss, C. I., and Wellman, T. P.: Influence of permafrost distribution
 957 on groundwater flow in the context of climate-driven permafrost thaw: Example
 958 from Yukon Flats Basin, Alaska, United States, Water Resour. Res. 48, W07524,
 959 doi:10.1029/2011WR011595, 2012.

960 Weiss N, Blok D, Elberling B, Hugelius G, Jørgensen CJ, Siewert MB, Kuhry P:
 961 Thermokarst dynamics and soil organic matter characteristics controlling initial
 962 carbon release from permafrost soils in the Siberian Yedoma region. Sedimentary
 963 Geology, <http://dx.doi.org/10.1016/j.sedgeo.2015.12.004>, 2015.

964 [Wetterich, S., Tumskey, V., Rudaya, N., Kuznetsov, V., Maksimov, F., Opel, T., Meyer,](#)
 965 [H., Andreev, A. A., and Schirrmeister, L.: Ice Complex permafrost of MIS5 age in](#)
 966 [the Dmitry Laptev Strait coastal region \(East Siberian Arctic\), Quaternary Science](#)
 967 [Reviews, 147, 298-311, 10.1016/j.quascirev.2015.11.016, 2016.](#)

968 Wiesenberg, G., Schwark, L., ~~and~~ Schmidt, M.: Improved automated extraction and
 969 separation procedure for soil lipid analyses. European Journal of Soil Science 55,
 970 349-356, 2014.

971 Wilkie, K.M.K., Chaplignin, B., Meyer, H., Burns, S., Petsch, S., and Brigham-Grette, J.:
 972 Modern isotope hydrology and controls on dD of plant leaf waxes at Lake
 973 El'gygytgyn, NE Russia, Clim. Past 9, 335-352, doi:10.5194/cp-9-335-2013, 2013.

974 Winterfeld, M., Lepple, T., and Mollenhauer, G.: Characterization of particulate
 975 organic matter in the Lena River delta and adjacent nearshore zone, NE Siberia –
 976 Part I: Radiocarbon inventories, Biogeosciences, 12, 3769-3788, doi:10.5194/bg-
 977 12-3769-2015, 2015.

978 Yang, H., Liu, W., Leng, Q., Hren, M.T., and Pagani, M.: Variation in n-alkane dD values
 979 from terrestrial plants at high latitude: implications for paleoclimate
 980 reconstruction, Org. Geochem. 42, 283-288,
 981 doi:10.1016/j.orggeochem.2011.01.006, 2011.

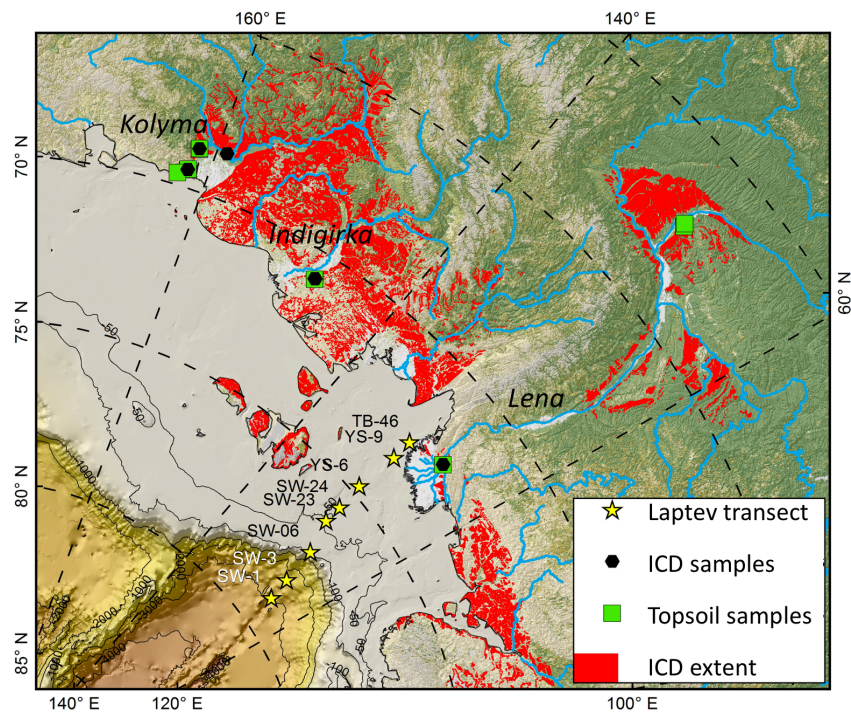
982 Zech, R., Huang, Y., Zech, M., Tarozo, R., and W. Zech: High carbon sequestration in
 983 Siberian permafrost loess-paleosols during glacials, Clim. Past, 7, 501-509,
 984 doi:10.5194/cp-7-501-2011, 2011.

985 Zimov, S.A., Semiletov, I. P. Daviodov, S. P., Voropaev, Y. V., Prosyannikov, S. F., Wong,
 986 C. S., and Y.-H. Chan: Wintertime CO₂ emission from soils of Northeastern Siberia.
 987 Arctic, 46, 197-204, 1993.

988

Deleted: ,
Deleted: 2004.
Deleted: .

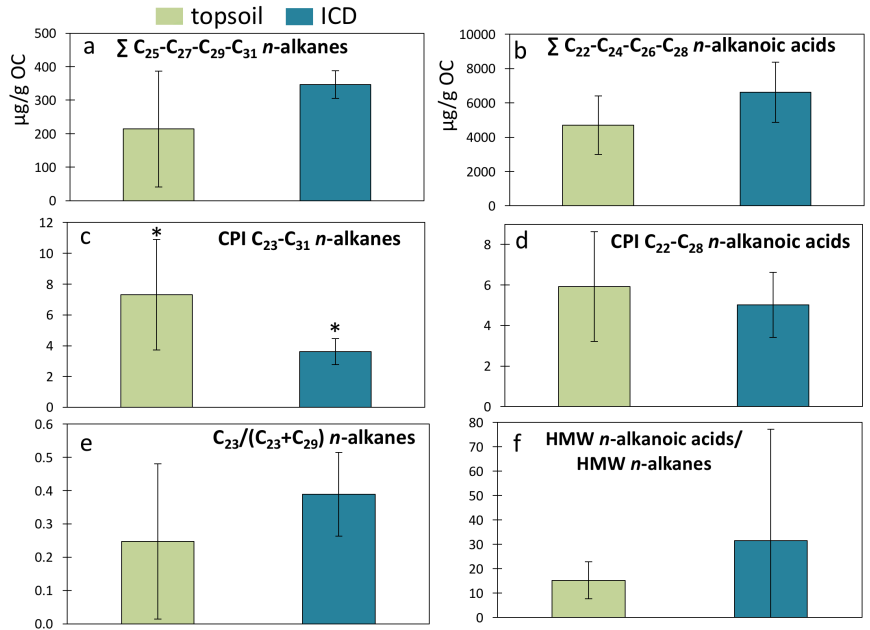
992 **Figure 1**
 993 Map of coastal northeast Siberia showing the extent of ice complex permafrost (ICD; red)
 994 overlaid with the location of ice complex (n=9; black diamonds) and topsoil samples
 995 (n=9; green squares). The shelf-slope Laptev Sea transect is shown with yellow stars.
 996
 997



998
 999

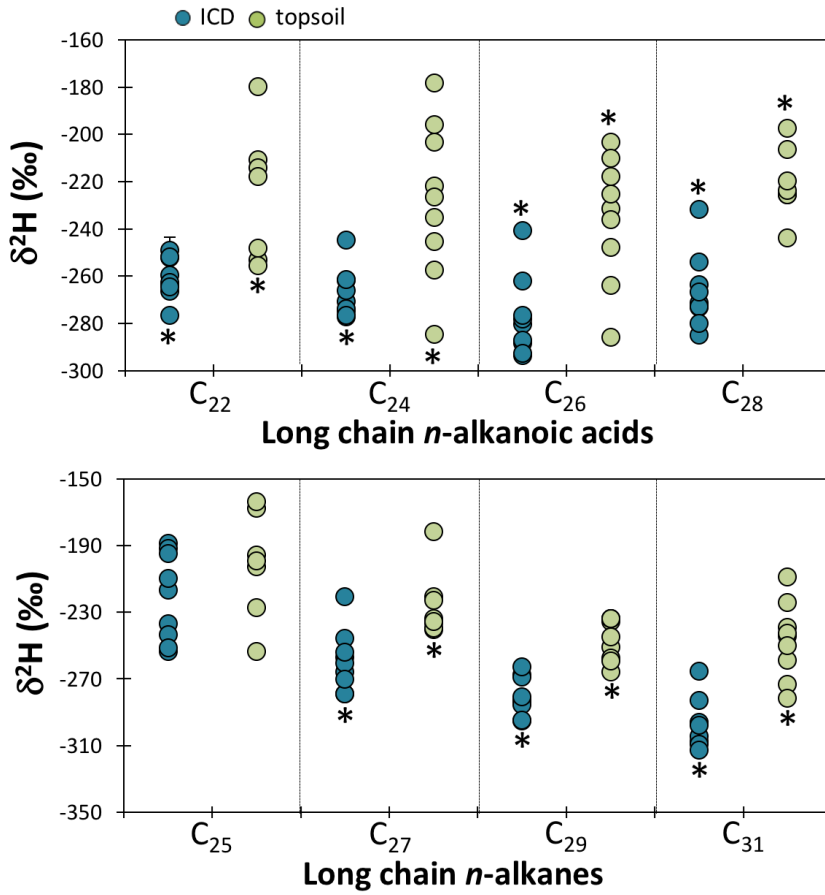
1000 **Figure 2**
 1001 Molecular concentrations and ratios of topsoil Holocene permafrost (green; $n=9$) and
 1002 deeper Pleistocene permafrost (blue; $n=9$) samples, with (a) the sum of odd n -alkanes
 1003 C_{25} - C_{31} , (b) the sum of even n -alkanoic acids C_{22} - C_{28} , (c) the Carbon Preference Index
 1004 (CPI) for n -alkanes C_{23} - C_{31} , (d), the CPI for n -alkanoic acids C_{22} - C_{28} , (e) the ratio of C_{23}
 1005 over $C_{23}+C_{29}$ n -alkanes, and (f) the sum of high-molecular weight (HMW) n -alkanoic
 1006 acids over HMW n -alkanes. The CPI is calculated as $CPI_{i-n} = \frac{1}{2} \frac{\sum (X_i+X_{i+2}+\dots+X_n)}{\sum (X_{i-1}+X_{i+1}+\dots+X_{n-1}) + \frac{1}{2} \sum (X_i+X_{i+2}+\dots+X_n)}$, where X is
 1007 concentration. Stars indicate that the two compared values are statistically significant
 1008 (95% confidence). Note that panel a and b are reported as median with IQR (interquartile
 1009 range) and the other panels are reported as average \pm standard deviation.
 1010
 1011

Deleted: 5
 Deleted: 5
 Deleted: ±



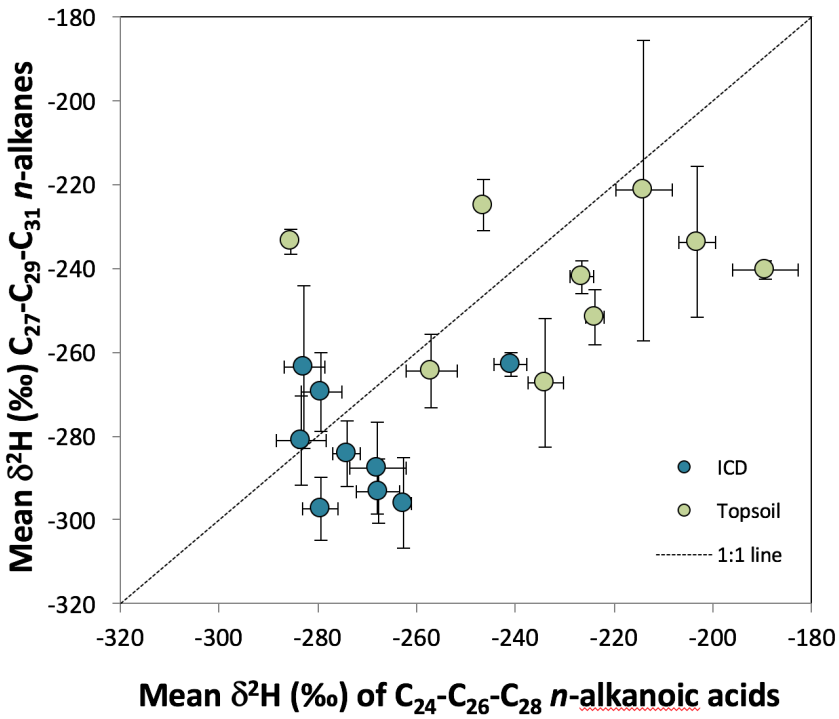
1012
 1013

1017 **Figure 3**
 1018 Molecular isotopic signature against chain length of long chain *n*-alkanoic acids (top) and
 1019 *n*-alkanes (bottom) for Holocene topsoil samples (green) and Pleistocene ice complex
 1020 samples (ICD; blue). Stars indicate that the two compared values are statistically
 1021 significant (95% confidence). Standard deviations are represented as vertical bars, and
 1022 are smaller than the sample circles when not visible.
 1023



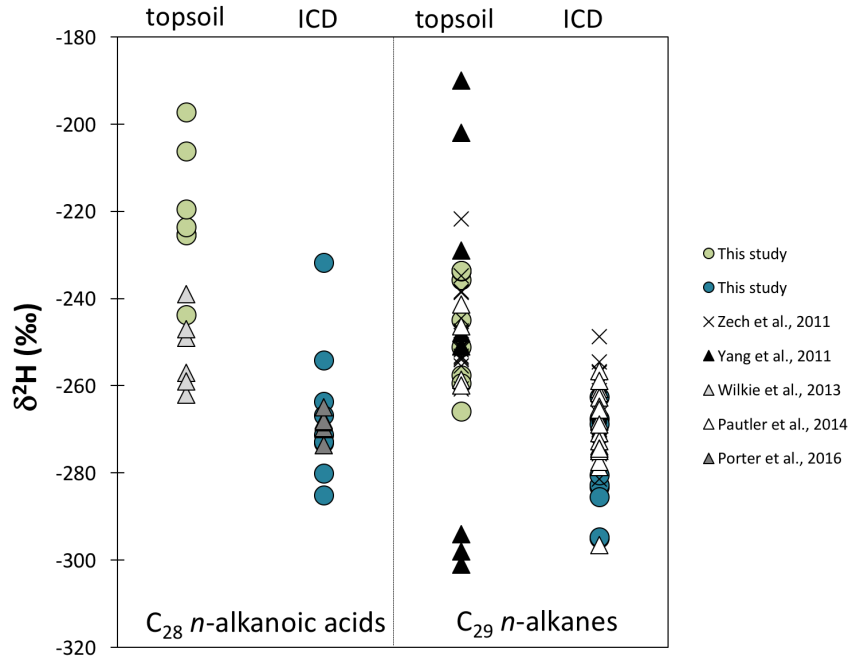
1024
 1025
 1026
 1027
 1028

1029 **Figure 4**
1030 Concentration-weighted mean $\delta^2\text{H}$ values of $\text{C}_{27}\text{-C}_{29}\text{-C}_{31}$ *n*-alkanes plotted against
1031 concentration-weighted mean $\delta^2\text{H}$ values of $\text{C}_{24}\text{-C}_{26}\text{-C}_{28}$ *n*-alkanoic acids to illustrate the
1032 fractionation differences between these two leaf wax markers. Dashed line indicates an
1033 identical fractionation.
1034



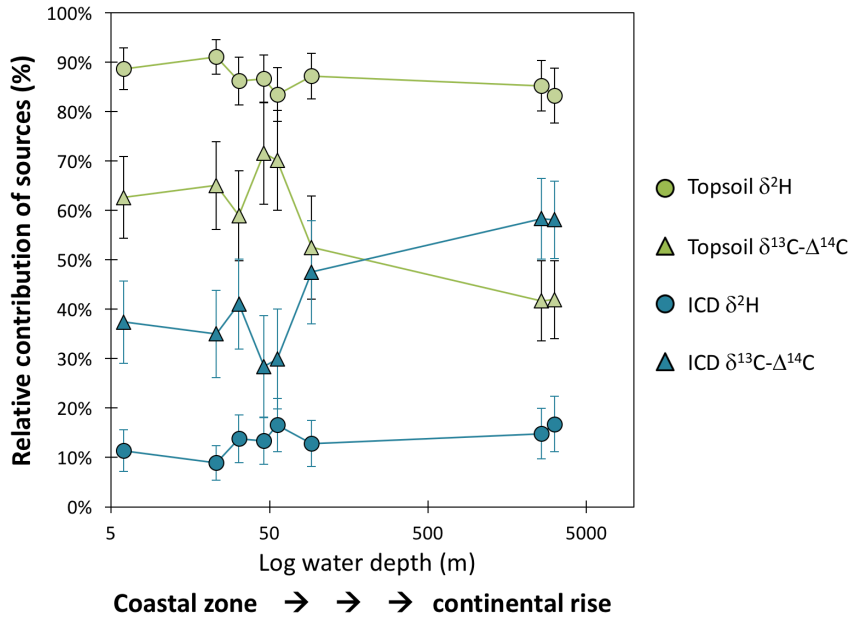
1035
1036

1037 **Figure 5**
 1038 Comparison of $\delta^2\text{H}$ values of C_{28} *n*-alkanoic acid (left) and C_{29} *n*-alkane (right) in
 1039 modern (Topsoil-PF; green circles) and ICD-PF for this study (blue circles) and
 1040 available literature, with crosses from Zech et al. (2011; glacial and interglacial
 1041 paleosoils from permafrost bluff exposure at Tumara River northeast Siberia), black
 1042 triangles from Yang et al. (2011; C3 plants and trees from Canada and Alaska), light
 1043 grey triangles from Wilkie et al. (2013; C3 plants from the El'gygytgyn lake basin,
 1044 Siberia), white triangles from Pautler et al. (2014; modern and paleosoils from the
 1045 Yukon territory, Canada) and dark grey triangles from Porter et al. (2016; muck
 1046 deposits from the Yukon territory, Canada).
 1047



1048
 1049
 1050
 1051

1052 **Figure 6**
 1053 Contribution of OC from Topsoil-PF (green) and ICD-PF (blue) sources to surface
 1054 sediments along a shelf-slope transect in the Laptev Sea (see also Bröder et al., 2016b for
 1055 further transect information), calculated with a $\delta^{13}\text{C}$ - $\Delta^{14}\text{C}$ (triangles) and leaf wax $\delta^2\text{H}$
 1056 mixing model (circles). Stations are plotted against log water depth (m; see also Table 6)
 1057 following the transect order from the coastal, nearshore, zone in the South (furthest left;
 1058 TB-46, 6 m depth) towards the continental rise in the North (furthest right; SW-01, 3146
 1059 m depth). Topsoil $\Delta^{14}\text{C}$ end-member values are corrected for cross-shelf transport time
 1060 (see section 4.2).
 1061



1062

Table 1

Site characteristics and geochemical properties of eight topsoil and eight ice complex deposit samples. A table with more detailed sample descriptions can be found in Supplementary Table 1.

Sample code	Sample ID	Current vegetation	Watershed	Description	Lat	Lon	TOC	$\delta^{13}\text{C}$	^{14}C yrs		
					°N	°E	%	‰	%	%	%
Topsoil (modern vegetation and O-horizon samples)											
TS-1	KU EXP 1-1, 0-16 cm	Tundra	Lena	Surface O-horizon; 0-16 cm	72.34	126.29	11	-27.0	n.a.	0.40	27.5
TS-2	CH YED2, 0-4 cm	Tundra	Kolyma	Surface O-A horizon; 0-4 cm	69.46	161.79	17	-28.4	n.a.	0.64	26.5
TS-3	SP T3-3B,	Alas grassland	Lena	Alas soil (Mollisol), mix of O and A horizon	62.32	129.50	15	-27.9	n.a.	1.40	10.7
TS-4	SP T2-7,	Larch taiga	Lena	Taiga soil (turbel), mix of O and A horizon	62.25	129.62	13	-28.4	n.a.	0.45	28.0
TS-5	KY T2-3,	Tussock tundra	Indigirka	Tundra soil (turbel), O-horizon	70.83	147.48	29	-28.5	n.a.	1.56	18.7
TS-6	CH T2-1,	Tussock tundra	Kolyma	Tundra soil (turbel), mix of O, Ojj and Ajj horizons	69.44	161.77	21	-26.4	n.a.	0.57	36.7
TS-7	CH YED3, 0-10 cm	Larch taiga	Kolyma	Surface O-hor; 0-10 cm	68.77	161.41	39	-29.6	n.a.	1.29	30.7
TS-8G ^a	CH Medv grass ^a	Grass tundra	Kolyma	Vegetation	69.64	162.54	41	-25.2	n.a.	Formatted: Superscript	
TS-9G ^a	CH Y4 grass ^a	Larch taiga	Kolyma	Vegetation	68.74	161.41	40	-28.5	n.a.	Formatted: Superscript	
Mean values							25	-27.8	1.1	24.8	
Ice complex deposits											
ICD-1	KU EXP 1-3, 212-216 cm	Tundra	Lena	Very deep undisturbed yedoma ca. 10 m below surface	72.34	126.29	1.3	-27.5	n.a.	0.08	15.7
ICD-2	CH YED1, 300-305 cm	Tussock tundra	Kolyma	Deep undisturbed yedoma ca. 3 m below surface	69.47	161.77	1.4	-26.3	n.a.	0.14	10.2
ICD-3	CH YED2, 300-305 cm	Tussock tundra	Kolyma	Deep undisturbed yedoma ca. 3 m below surface	69.46	161.79	2.3	-25.8	n.a.	0.27	8.6
ICD-4	CH YED3, 520-525 cm	Larch taiga	Kolyma	Deep undisturbed yedoma ca. 5 m below surface	68.77	161.41	1.4	-25.5	n.a.	0.15	9.7
ICD-5	KY EXP1, 0-5 cm	Tussock tundra	Indigirka	Undisturbed yedoma ca. 2 m below surface	70.83	147.44	1.5	-25.5	27920	0.18	8.5
ICD-6	KY EXP2, 110-115 cm	Tussock tundra	Indigirka	Deep undisturbed yedoma ca. 4.5 m below surface	70.83	147.44	1.6	-25.6	17270	0.19	8.6
ICD-7	KY EXP3, 185-190 cm	Tussock tundra	Indigirka	Undisturbed yedoma ca. 2 m below surface	70.83	147.49	1.5	-25.2	±210 ±80	0.17	8.5

<u>ICD-8</u>	CH DY-3A	Larch taiga	Kolyma	Particulate matter from thaw streams	68.63	159.15	1.5 ^b	-25.2 ^b	<u>19370</u>	-	-
<u>ICD-9</u>	CH DY-4A	Larch taiga	Kolyma	Particulate matter from thaw streams	68.63	159.15	1.4 ^b	-25.1 ^b	<u>28040</u>	-	-
	Mean values						1.6	-25.7	0.2	10.0	

a vegetation/grass samples, labelled with "G"

b data from Vonk et al., 2013

Table 2

Long-chain *n*-alkane concentrations (in µg/gOC) of topsoil Holocene samples (modern vegetation/O-horizon) and Pleistocene ice complex samples.

	C21	C22	C23	C24	C25	C26	C27	C28	C29	C30	C31	C32	C33
	µg/g OC												
Topsoil (modern vegetation and O-horizon samples)													
<u>TS-1</u>	44	88	96	45	41	10	45	4.4	27	2.5	36	1.5	7.2
<u>TS-2</u>	24	15	21	12	40	10	160	10	150	6.5	150	3.5	17
<u>TS-3</u>	2.5	2.4	5.9	2.6	13	4.7	42	16	74	4.7	85	2.7	24
<u>TS-4</u>	19	3.3	7.1	2.7	27	4.5	47	6.7	98	9.1	150	5.7	38
<u>TS-5</u>	35	8.4	26	9.9	38	13	91	18	180	14	230	8.1	43
<u>TS-6</u>	14	5.1	16	5.7	19	4.0	26	3.7	48	5.0	120	4.0	32
<u>TS-7</u>	46	12	18	8.8	22	16	61	27	220	23	340	12	48
<u>TS-8G</u>	4.1	1.7	18	10	61	16	47	13	30	5.3	10	1.1	1.1
<u>TS-9G</u>	4.7	2.6	18	15	45	21	50	16	31	6.8	9.8	1.5	2.6
Ice complex deposits													
<u>JCD-1</u>	57	79	100	49	82	23	170	16	137	8.5	140	4.4	25
<u>JCD-2</u>	55	89	100	70	70	27	75	20	130	12	120	5.3	28
<u>JCD-3</u>	40	64	74	31	54	15	79	22	110	10	160	4.8	32
<u>JCD-4</u>	60	93	98	47	55	20	84	22	140	12	150	6.0	39
<u>JCD-5</u>	46	79	86	56	49	20	55	13	75	7.0	100	4.7	38
<u>JCD-6</u>	41	73	87	68	62	29	65	20	98	11	120	4.9	27
<u>JCD-7</u>	50	83	83	43	41	16	65	17	100	8.3	120	4.5	42
<u>JCD-8</u>	4.2	7.3	23	30	55	42	82	38	100	18	110	5.0	21
<u>JCD-9</u>	6.2	6.2	16	11	29	15	51	20	79	9.3	85	4.1	23

Deleted: KU EXP 1-1, 0-16 cm**Deleted:** CH YED2, 0-4 cm**Deleted:** SP T3-3B**Deleted:** SP T2-7**Deleted:** KY T2-3**Deleted:** CH T2-1**Deleted:** CH YED3, 0-10 cm**Deleted:** CH Medv grass**Deleted:** CH Y4 grass**Deleted:** KU EXP 1-3, 212-216 cm**Deleted:** CH YED1, 300-305 cm**Deleted:** CH YED2, 300-305 cm**Deleted:** CH YED3, 520-525 cm**Deleted:** KY EXP1, 0-5 cm**Deleted:** KY EXP2, 110-115 cm**Deleted:** KY EXP3, 185-200 cm**Deleted:** CH DY-3A**Deleted:** CH DY-4A

Table 3

Long-chain *n*-alkanoic acids concentrations (in µg/gOC) of topsoil Holocene samples (modern vegetation/O-horizon) and Pleistocene ice complex samples.

	C16	C18	C20	C21	C22	C23	C24	C25	C26	C27	C28	C29	C30	
	µg/gOC													
Topsoil (modern vegetation and O-horizon samples)														
TS-1	511	220	176	80.5	539	311	1100	4.95	684	90.5	350	32.8	58.1	Deleted: KU EXP 1-1, 0-16 cm
TS-2	1740	664	673	235	1380	496	1390	543	1740	409	1580	113	305	Deleted: CH YED2, 0-4 cm
TS-3	664	296	480	116	1020	504	1710	415	1550	250	1060	132	456	Deleted: SP T3-3B
TS-4	1140	408	665	235	1400	431	1410	425	1250	242	651	143	455	Deleted: SP T2-7
TS-5	513	343	530	133	1140	359	1410	1.58	896	119	494	67.8	224	Deleted: KY T2-3
TS-6	1080	537	418	236	1420	790	2670	2.82	1570	127	657	46.6	174	Deleted: CH T2-1
TS-7	1420	352	538	281	1850	722	2010	651	1790	642	1580	730	1971	Deleted: CH YED3, 0-10 cm
TS-8G	3640	855	691	44.1	609	63.5	156	26.0	224	0.122	99.3	9.91	28.1	Deleted: CH Medv grass
TS-9G	4600	887	966	53.6	815	66.7	261	28.6	232	11.5	124	8.10	30.2	Deleted: CH Y4 grass
Ice complex deposits														
ICD-1	1750	1600	4560	1460	9460	2300	8930	2020	5830	1030	3660	293	635	Deleted: KU EXP 1-3, 212-216 cm
ICD-2	10400	4030	5800	2410	17100	7270	18600	6610	16600	5860	14800	6810	18700	Deleted: CH YED1, 300-305 cm
ICD-3	665	554	892	263	2070	1060	3070	646	2340	272	1310	133	532	Deleted: CH YED2, 300-305 cm
ICD-4	1400	769	1030	252	2040	910	3120	644	2440	266	1160	124	432	Deleted: CH YED3, 520-525 cm
ICD-5	426	304	447	126	1220	511	1970	70.4	1390	133	712	60.7	233	Deleted: KY EXP1, 0-5 cm
ICD-6	722	539	583	153	1370	606	2270	457	1970	181	1030	86.4	333	Deleted: KY EXP2, 110-115 cm
ICD-7	446	313	543	158	1330	562	2350	401	1370	154	743	63.1	230	Deleted: KY EXP3, 185-200 cm
ICD-8	920	402	895	108	1070	294	1180	184	799	70.3	331	34.4	100	Deleted: CH DY-3A
ICD-9	327	200	559	74	803	229	1010	2.17	718	64.9	334	28.7	104	Deleted: CH DY-4A

Table 4

Sum of most abundant long-chain *n*-alkanoic acids and *n*-alkanes (concentrations in µg/gOC), and characteristic ratios of *n*-alkanoic acids and *n*-alkanes of topsoil Holocene (modern vegetation/O-horizon) and Pleistocene ice complex samples.

	<i>n</i> -alkanoic acids			HMW acids/ HMW alkanes ^a	<i>n</i> -alkanes			C ₂₃ / (C ₂₃ +C ₂₃) ^c	C ₂₅ / (C ₂₅ +C ₂₉)
	ΣHMW ^a (>C ₂₂) µg/gOC	ΣC ₂₂ -C ₂₈ (even) µg/gOC	CPI ^b		ΣHMW ^a (>C ₂₁) µg/gOC	ΣC ₂₅ -C ₃₁ (odd) µg/gOC	CPI ^c		
Topsoil (modern vegetation and O-horizon samples)									
TS-1 _v	3167	2670	5.8	7.1	447	148	2.7	0.78	0.60
TS-2 _v	7958	6090	3.8	13	612	494	11	0.12	0.21
TS-3 _v	7095	5340	4.1	25	280	214	7.2	0.07	0.15
TS-4 _v	6397	4700	3.7	15	418	323	12	0.07	0.24
TS-5 _v	4715	3940	6.8	6.6	717	543	9.1	0.12	0.17
TS-6 _v	7454	6310	6.0	25	300	211	9.9	0.25	0.28
TS-7 _v	11950	7230	2.9	14	857	647	7.8	0.08	0.09
TS-8 _G	1216	1090	9.5	5.6	217	148	3.7	0.37	0.67
TS-9 _G	1577	1430	11	7.1	223	135	2.5	0.36	0.59
Mean±stdev	5726±3431	4310±2190	5.9	13	452±230	318±195	7.3	0.25	0.33
Median and IQR	6397 ⁷⁴⁵⁴ ₃₁₆₇	4700 ⁶³¹⁰ ₆₀₉₂	2.7	7.6	418 ⁶²¹ ₂₈₀	214 ⁴⁹⁴ ₁₄₈	3.6	0.23	0.22
Ice complex deposits									
ICD-1 _v	34854	27883	4.1	39	893	530	4.9	0.43	0.38
ICD-2 _v	112356	67078	2.8	140	806	398	3.0	0.44	0.35
ICD-3 _v	11430	8791	4.1	16	698	405	4.6	0.40	0.33
ICD-4 _v	11145	8768	4.4	14	825	428	3.8	0.42	0.29
ICD-5 _v	6293	5285	6.5	10	630	280	2.9	0.54	0.40
ICD-6 _v	8293	6629	4.9	12	708	347	2.7	0.47	0.39
ICD-7 _v	7196	5787	4.7	11	671	323	3.5	0.45	0.29
ICD-8 _v	4063	3380	5.5	7.6	533	344	2.7	0.19	0.35
ICD-9 _v	3295	2867	8.3	9.3	355	244	4.3	0.17	0.27
Mean±stdev	22103±35150	15160±20800	5.0	29	680±163	367±85	3.6	0.39	0.34
Median and IQR	8290 ¹¹⁴³⁰ ₆₂₉₀	6630 ⁸⁷⁹⁰ ₅₂₈₅	1.6	43	698 ⁸⁰⁶ ₆₃₀	347 ⁴⁰⁵ ₃₂₃	0.8	0.13	0.05

a HMW; high-molecular weight

b CPI; carbon preference index for chain lengths C₂₂-C₂₈, for calculation see caption of Fig. 2.

c CPI; carbon preference index for chain lengths C₂₃-C₃₁, for calculation see caption of Fig. 2.

Deleted: KU EXP 1-1, 0-16 cm
Deleted: CH YED2, 0-4 cm
Deleted: SP T3-3B
Formatted Table
Deleted: SP T2-7
Deleted: KY T2-3
Deleted: CH T2-1
Deleted: CH YED3, 0-10 cm
Deleted: CH Medv grass
Deleted: CH Y4 grass
Deleted: (6397)
Deleted: (4700)
Deleted: (418)
Deleted: (214)
Formatted Table
Deleted: (median)
Deleted: St.dev ...edian and (...QR)
Deleted: 3431 (4290)
Deleted: 2190 (4320)
Deleted: 230
Deleted: 195 (345)
Deleted: KU EXP 1-3, 212-216 cm
Deleted: CH YED1, 300-305 cm
Deleted: CH YED2, 300-305 cm
Deleted: CH YED3, 520-525 cm
Deleted: KY EXP1, 0-5 cm
Deleted: KY EXP2, 110-115 cm
Deleted: KY EXP3, 185-200 cm
Deleted: CH DY-3A
Deleted: CH DY-4A
Deleted: (8290)
Deleted: (6630)
Deleted: (698)
Deleted: (347)
Formatted Table
Deleted: 35150(5140)
Deleted: 20880 (3510)
Deleted: 163 (176)
Deleted: 85 (81)
Deleted: St.dev

Table 5

$\delta^2\text{H}$ signatures (in ‰) of *n*-alkanoic acids and *n*-alkanes of topsoil Holocene (modern vegetation/O-horizon) and Pleistocene ice complex samples.

	<i>n</i> -alkanoic acids							<i>n</i> -alkanes			
	C16	C18	C20	C22	C24	C26	C28	C25	C27	C29	C31
Topsoil (modern vegetation and O-horizon samples)											
TS-1	-162	-180		-119	-178	-203	-197	-168	-240	-236	-244
TS-2	-188	-192		-211	-222	-232	-225	-196	-237	-251	-239
TS-3				-126	-203	-218	-225		-125	-234	-259
TS-4	-171	-213		-180	-196	-210	-206		-182	-245	-243
TS-5		-235	-185	-253	-257	-264	-244	-164	-240	-266	-273
TS-6	-189	-222		-214	-235	-236	-224	-203	-221	-258	-282
TS-7	-184		-190	-218	-227	-225	-220	-199	-234	-259	-250
TS-8G	-258	-246	-253	-256	-285	-286		-253	-236	-234	-224
TS-9G	-237	-244	-251	-248	-245	-248		-227	-223	-234	-209
Mean	-199	-219	-220	-203	-228	-236	-220	-201	-215	-246	-247
St.dev	35	25	37	52	33	27	15	32	39	13	23
Ice complex deposits											
ICD-1	-194	-227	-243	-252	-245	-241	-232	-237	-257	-268	-265
ICD-2			-231	-264	-271	-280	-271	-217	-266	-283	-297
ICD-3				-249	-262	-278	-264	-254	-279	-283	-307
ICD-4			-209	-252	-266	-277	-254	-243	-261	-285	-305
ICD-5			-169	-260	-275	-288	-273	-189	-245	-269	-283
ICD-6	-211	-216	-252	-266	-274	-294	-285	-192	-254	-281	-296
ICD-7			-191	-263	-277	-287	-273	-210	-279	-295	-309
ICD-8	-244	-256	-277	-277	-277	-293	-280	-195	-221	-263	-298
ICD-9	-228	-229	-261	-265	-262	-262	-267	-251	-270	-295	-313
Mean	-219	-232	-229	-261	-268	-278	-267	-221	-259	-280	-297
St.dev	21	17	37	8.6	10	17	16	26	18	12	15

Deleted: KU EXP 1-1, 0-16 cm
Deleted: CH YED2, 0-4 cm
Deleted: SP T3-3B
Deleted: SP T2-7
Deleted: KY T2-3
Deleted: CH T2-1
Deleted: CH YED3, 0-10 cm
Deleted: CH Medv grass
Deleted: CH Y4 grass

Deleted: KU EXP 1-3, 212-216 cm
Deleted: CH YED1, 300-305 cm
Deleted: CH YED2, 300-305 cm
Deleted: CH YED3, 520-525 cm
Deleted: KY EXP1, 0-5 cm
Deleted: KY EXP2, 110-115 cm
Deleted: KY EXP3, 185-200 cm
Deleted: CH DY-3A
Deleted: CH DY-4A

Table 6

Location, sampling depth and isotopic values of samples along a surface sediment transect in the Laptev Sea (data from Bröder et al., 2016b), with percentage topsoil (TS) and ice complex deposit (ICD) OC contributions to the samples based on source-apportionment calculations with $\delta^2\text{H}$ leaf wax end-members versus $\delta^{13}\text{C}-\Delta^{14}\text{C}$ end-members (end-member values are described in the text).

ID ^a	Lat N	Long °E	Depth m	Sample values						Source contributions			
				C ₂₇ ‰	C ₂₉ ‰	C ₃₁ ‰	C ₂₇₋₂₉₋₃₁ ^b ‰	$\delta^{13}\text{C}$ ‰	$\Delta^{14}\text{C}$ ‰	TS using $\delta^2\text{H}$	ICD using $\delta^2\text{H}$	TS ^c using $\delta^{13}\text{C}-\Delta^{14}\text{C}$	ICD ^c using $\delta^{13}\text{C}-\Delta^{14}\text{C}$
TB-46	72.700	130.180	6	-236.2	-237.4	-230.4	-235.0	-26.5	-436	89%	11%	63% (63%)	37% (37%)
YS-9	73.366	129.997	23	-233.7	-231.0	-227.8	-231.1	-26.1	-415	91%	8.9%	63% (65%)	37% (35%)
YS-6	74.724	130.016	32	-234.2	-241.0	-235.4	-236.8	-25.6	-465	86%	14%	51% (59%)	49% (41%)
SW-24	75.599	129.558	46	-229.3	-236.5	-243.5	-236.4	-24.8	-284	87%	13%	70% (72%)	30% (28%)
SW-23	76.171	129.333	56	-219.9	-243.3	-243.3	-236.0	-25.0	-333	83%	17%	65% (70%)	35% (30%)
SW-06	77.142	127.378	92	-219.5	-237.0	-241.4	-233.2	-23.2	-364	87%	13%	39% (53%)	61% (47%)
SW-03	78.238	126.150	2601	-221.1	-238.0	-247.7	-235.9	-22.6	-426	85%	15%	23% (42%)	77% (58%)
SW-01	78.942	125.243	3146	-223.8	-241.8	-246.0	-238.0	-22.3	-418	83%	17%	21% (42%)	79% (58%)

a Location, depth and bulk carbon isotope data from Bröder et al. (2016b)

b weighted average based on individual concentrations

c numbers in brackets are source contributions using the $\delta^{13}\text{C}-\Delta^{14}\text{C}$ approach but with additional corrections for cross-shelf lateral transport time of topsoil OC (similar as in Bröder et al., 2016a); we applied linear aging along the transect based on the distance from the coast, with a maximum aging of 5000 years for station SW-01.

Page 32: [1] Formatted Table	Jorien	5/25/17 9:04:00 AM
Formatted Table		
Page 32: [2] Formatted Table	Jorien	5/25/17 9:05:00 AM
Formatted Table		
Page 32: [3] Formatted Table	Jorien	6/3/17 3:00:00 PM
Formatted Table		
Page 32: [4] Deleted	Jorien	6/3/17 2:59:00 PM
<i>St.dev</i>		
Page 32: [4] Deleted	Jorien	6/3/17 2:59:00 PM
<i>St.dev</i>		
Page 32: [4] Deleted	Jorien	6/3/17 2:59:00 PM
<i>St.dev</i>		
Page 32: [5] Formatted Table	Jorien	6/3/17 3:11:00 PM
Formatted Table		